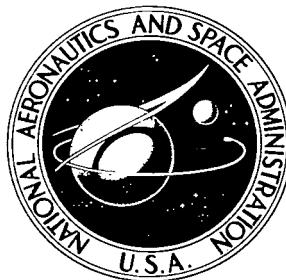


NASA TECHNICAL NOTE



NASA TN D-5645

2.1

NASA TN D-5645



LOAN COPY: RETURN TO
AFWL (WLOL)
KIRTLAND AFB, N MEX

THERMOMECHANICAL PROCESSING OF MOLYBDENUM-HAFNIUM-CARBON ALLOYS

by Peter L. Raffo

*Lewis Research Center
Cleveland, Ohio*



NATIONAL AERONAUTICS AND SPACE ADMINISTRATION • WASHINGTON, D. C. • FEBRUARY 1970



0132463

1. Report No. NASA TN D-5645	2. Government Accession No.	3. Recipient's Catalog No.
4. Title and Subtitle THERMOMECHANICAL PROCESSING OF MOLYBDENUM-HAFNIUM-CARBON ALLOYS		5. Report Date February 1970
7. Author(s) Peter L. Raffo		6. Performing Organization Code
9. Performing Organization Name and Address Lewis Research Center National Aeronautics and Space Administration Cleveland, Ohio 44135		8. Performing Organization Report No. E-5297
12. Sponsoring Agency Name and Address National Aeronautics and Space Administration Washington D. C. 20546		10. Work Unit No. 129-03
15. Supplementary Notes		11. Contract or Grant No.
16. Abstract A study was made of the thermochemical processing of a series of Mo-Hf-C alloys. The processes either produced an overaged carbide precipitate within a strain hardened matrix or allowed the formation of a finer precipitate during fabrication by a dynamic strain aging reaction. The short time tensile properties of the strain aged alloys were superior to those of any other molybdenum alloy studied to date.		13. Type of Report and Period Covered Technical Note
17. Key Words (Suggested by Author(s)) Thermomechanical processing Molybdenum alloys Carbide strengthening	18. Distribution Statement Unclassified - unlimited	14. Sponsoring Agency Code
19. Security Classif. (of this report) Unclassified	20. Security Classif. (of this page) Unclassified	21. No. of Pages 47
		22. Price* \$3.00

*For sale by the Clearinghouse for Federal Scientific and Technical Information
Springfield, Virginia 22151

THERMOMECHANICAL PROCESSING OF MOLYBDENUM- HAFNIUM-CARBON ALLOYS

by Peter L. Raffo
Lewis Research Center

SUMMARY

A study was made of the thermomechanical processing of a series of molybdenum-hafnium-carbon (Mo-Hf-C) alloys. The hafnium content was varied from 0.47 to 1.09 percent, while the carbon content was varied from 0.29 to 1.19 percent (all compositions in atom percent). One type of processing schedule involved different annealing treatments prior to the final swaging. These, in general, produced an overaged HfC precipitate within a strain hardened matrix. The short time tensile strength of these alloys depended on the subgrain size and the particle size and spacing. The minimum creep rate at 2400^o F (1588 K) was found to be proportional to $L^{2.9}$, where L is the interparticle spacing of the HfC.

Another type of process was developed in which a metastable alloy is swaged under conditions where precipitation occurs during deformation, a form of dynamic strain aging. One such alloy, Mo-0.6 percent Hf-0.5 percent C had an ultimate tensile strength greater than 100 ksi (690 MN/m²) over the temperature range 1500^o to 2700^o F (1088 to 1766 K).

In addition to the studies on Mo-Hf-C alloys, a commercial molybdenum-titanium-zirconium-carbon alloy (Mo-TZC) was solution treated and then hydrostatically extruded at room temperature. The limited data obtained on this highly cold-worked material showed it to have an excellent combination of short time tensile strength and long term creep resistance at 2400^o F (1588 K).

INTRODUCTION

Much of the recent research on molybdenum has been concerned with the development of useful high strength alloys (refs. 1 to 3). Two important conclusions have arisen from this work. First, molybdenum alloys strengthened by carbides of titanium and zirconium possess the most useful combination of high-temperature strength and

low-temperature ductility. Second, the entire thermomechanical history of a given alloy is extremely important in determining its final mechanical properties. Previous studies at the Lewis Research Center have identified an analogous series of tungsten alloys strengthened by hafnium carbide (refs. 4 and 5). These alloys possess a high-temperature strength superior to any other refractory material above 3000⁰ F (1922 K). Because of the higher thermodynamic stability of hafnium carbide over titanium or zirconium carbide, it was decided to study the properties of Mo-Hf-C alloys as well.

Results of the preliminary evaluation of Mo-Hf-C alloys from this laboratory were presented earlier (ref. 6). In that study, the hafnium and carbon contents were varied over a wide range while processing differences were kept to a minimum. Some outstanding mechanical properties were developed in a few of the alloys which were comparable to those of the best molybdenum alloys developed in other laboratories. However, in spite of the attempt to avoid the processing history as a variable, it was obvious that the alloys were responding differently to the chosen processing schedule. The present work was initiated in order to characterize more thoroughly the effects of processing variables on the structure and properties of Mo-Hf-C alloys.

The mechanical properties of five Mo-Hf-C alloys have been measured after subjecting them to a series of controlled thermomechanical processing treatments. The alloys selected for this study contained 0.47 to 1.09 percent Hf and 0.29 to 1.19 percent C (all compositions in atom percent). After swaging to rod with selected intermediate anneals, the alloys were evaluated by tensile tests at room temperature and 1500⁰ to 3000⁰ F (1088 to 1922 K) and creep rupture tests at 2400⁰ F (1588 K). Room-temperature hydrostatic extrusion was utilized in the processing of a commercial Mo-TZC alloy. The data collected from the extrusion were compared with data for Mo-TZC processed by more conventional means. The microstructures of all the alloys were studied using transmission electron microscopy and were correlated with the mechanical properties.

EXPERIMENTAL PROCEDURES

Tables I and II list the compositions and processing conditions for the alloys investigated.

Consolidation and Fabrication

Elemental molybdenum, hafnium, and carbon powders were blended, hydrostatically pressed into 1-inch- (2.54-cm-) diameter electrodes, and vacuum sintered at 2800⁰ F

(1810 K). The alloys were vacuum melted in a consumable-arc melting furnace into 2.5-inch- (6.25-cm-) diameter ingots.

The ingots were then machined to 2 inches (5.08 cm) in diameter and extruded at an eight-to-one reduction ratio at either 3500^o or 4000^o F (2200 or 2477 K). Reference 7 may be consulted for details of the extrusion process. The extruded bars were thermomechanically processed according to the schedules outlined in table II. Chemical analyses for hafnium and carbon were obtained on the swaged rods.

A commercial alloy, Mo-TZC (Mo-2.4 percent Ti-0.18 percent Zr-0.88 percent C) was obtained as 0.75-inch- (1.9-cm-) diameter bar for thermomechanical processing based on cold hydrostatic extrusion. The bar was swaged at 2500^o F (1644 K) to a diameter of 0.4 inch (1 cm) and an extrusion billet 3.5 inches (8.9 cm) long with a 40^o cone angle was prepared. The billet was first solution treated at 4000^o F (2477 K) for 30 minutes and helium quenched. It was then coated with a commercial polymeric coating and extruded at room temperature in a fluid-to-fluid hydrostatic extrusion press of the type described by Bobrowsky and Stack (ref. 8). The fluid used was a one-to-one mixture of gasoline and castor oil. The billet was given a 60-percent reduction requiring a differential pressure of 237 ksi (1640 MN/m²).

Annealing

Annealing at temperatures at or below 3000^o F (1922 K) was performed by induction heating in hydrogen using a tungsten susceptor. Annealing treatments above 3000^o F (1922 K) were conducted at pressures less than 5×10^{-5} torr in a vacuum furnace which was modified to allow quenching of the specimen by the introduction of cold helium gas. Decarburization was maintained below 10 percent during solution annealing at 4000^o F (2477 K) by the presence of a few grams of molybdenum carbide (Mo₂C).

Mechanical Testing

Tensile specimens were centerless ground from the swaged rod according to the configurations in figure 1. Specimens for room-temperature tests were electropolished in 98-percent sulfuric acid prior to testing; tests above 1500^o F (1088 K) were performed on specimens in the as-ground condition. Tensile tests were performed at a pressure of less than 5×10^{-5} torr in the temperature range 1500^o to 3000^o F (1088 to 1922 K) and at a strain rate of 0.05 per minute. Creep rupture tests at 2400^o F (1588 K) were conducted in a commercial unit equipped with a tungsten mesh heating element. Creep deformation was followed by a dial gage attached to the load train. The dial gage was periodically photographed to record the deformation.

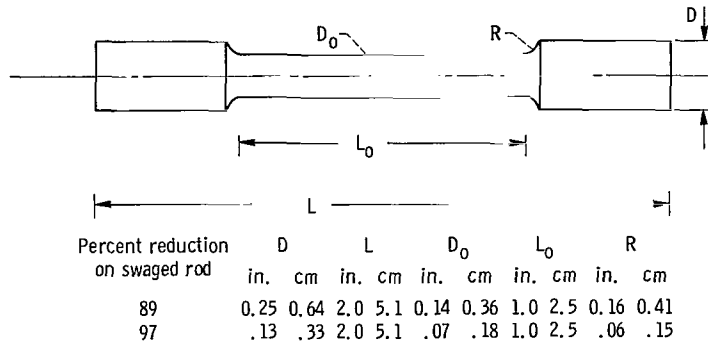


Figure 1. - Tensile specimen dimensions.

Metallography

Particle size and spacing were measured on direct carbon surface replicas of selected alloys. The specimens were initially electropolished in a 12.5-percent solution of sulfuric acid in methyl alcohol. They were then etched with an alkaline potassium ferrocyanide solution. The particle diameters were measured using a commercial particle counter. A mean planar particle diameter $2r_s$ was computed from the distribution. From 300 to 500 particles were counted for each alloy. The particle diameters ranged from 0.09 to 0.3 micrometer. The interparticle spacing was obtained by first calculating the mean planar center-to-center particle spacing λ from the equation (ref. 9)

$$\lambda = \frac{4}{\pi} \sqrt{\frac{1}{N_a}}$$

where N_a is the number of particles intersecting a unit area. The interparticle spacing L was then calculated from the expression

$$L = \lambda - 2r_s$$

Thin foils were prepared for transmission electron microscopy from 0.125-inch- (0.32-cm-) diameter disks which were spark machined from either the swaged rod or the reduced sections of tensile specimens. The disks were ground to a thickness of 0.2 to 0.5 millimeter and thinned electrolytically in a solution of 12.5-percent sulfuric acid in ethyl alcohol at 30 volts and 40° F (275 K) using a double jet apparatus of the type described by Schoone and Fischione (ref. 10). The foils were subsequently examined at 100 kilovolts.

RESULTS

Fabrication

The compositions and processing conditions for the alloys are listed in tables I and II. The rationale for choosing these particular processes is as follows: Process A is nearly identical to that used in the previous study (ref. 6) and is employed here for comparison with that work. Processes B, E, F, G, and L all involve the production of a solution treated and fully aged structure prior to swaging. This process is identical to that found successful with other carbide strengthened molybdenum alloys (refs. 1 and 3). Processes C, D, and K are all directed toward producing a fine carbide distribution by allowing precipitation to occur during deformation by swaging. This is accomplished in processes C and D by solution treating the extrusion prior to swaging. In process K, the ingot was extruded from 4000^o F (2477 K). The Mo-C binary phase diagram (refs. 11 and 12) is shown in figure 2. It was shown previously by the author (ref. 6) that this diagram approximates as a (Mo-Hf)-C pseudobinary for hafnium contents up to 1.8 percent. It can be seen from figure 2 that, at 4000^o F (2477 K), all carbides would be expected to be in solid solution.

All the preceding processing conditions produced some sound material with the exception of process C as applied to MHC-41, Mo-0.99 percent Hf-0.72 percent C. Process

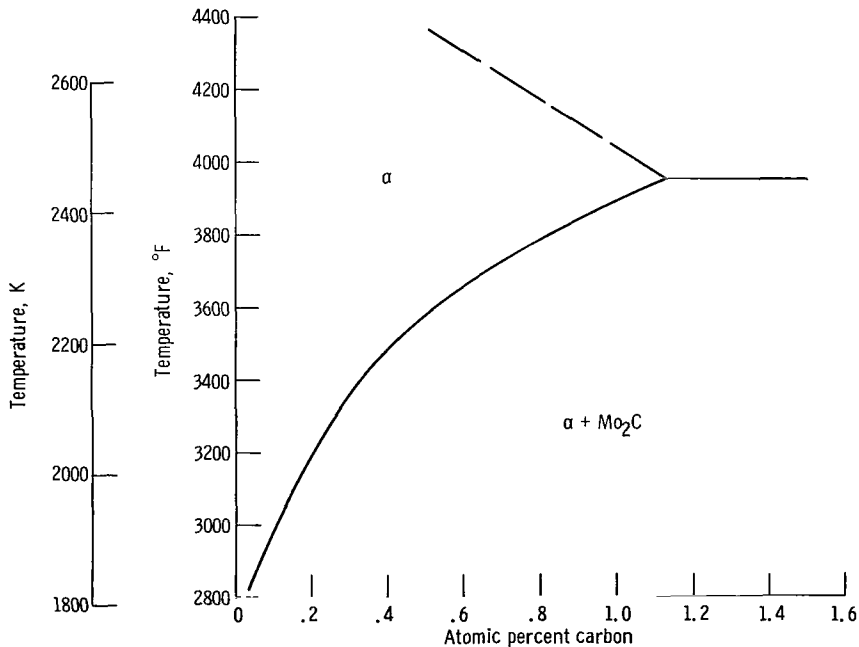


Figure 2. - Portion of molybdenum-carbon binary phase diagram (refs. 11 and 12).

C was also designed to allow precipitation of carbides during swaging by preceding the swaging with a 4000⁰ F (2477 K) solution anneal. However, the extrusion cracked on the second swaging pass. Similar results were found for analogous treatments on Mo-Ti-Zr-C alloys (ref. 1).

Throughout this report, each specific material is identified by a code which includes the alloy composition and processing treatment. For example, MHC-38E-89 refers to the composition MHC-38 (see table I), the process E (see table II), and the total percent reduction during swaging (89 percent).

Annealing Behavior

Table III lists the 1-hour recrystallization temperature T_r for a representative group of the alloys. The value of T_r is defined as the temperature for a two-thirds decrease in hardness from the as-swaged to the fully recrystallized values (ref. 6). The recrystallization temperatures varied from 2640⁰ to 3250⁰ F (1722 to 2061 K). The value of T_r was generally highest for those alloys processed in the E and L conditions, that is, where a fully aged structure was present prior to swaging.

The annealing behavior of alloy MHC-38E-89, Mo-0.47 percent Hf-0.29 percent C, was examined in detail. Tensile specimens and disks for transmission electron microscopy were annealed with the samples for hardness measurements. The tensile specimens were tested in creep rupture; these results are discussed in a later section. A plot of the room-temperature hardness as a function of annealing temperature is given in figure 3. A large hardness decrease typical of primary recrystallization was seen after annealing above 3000⁰ F (1922 K). Transmission electron microscopy showed that little

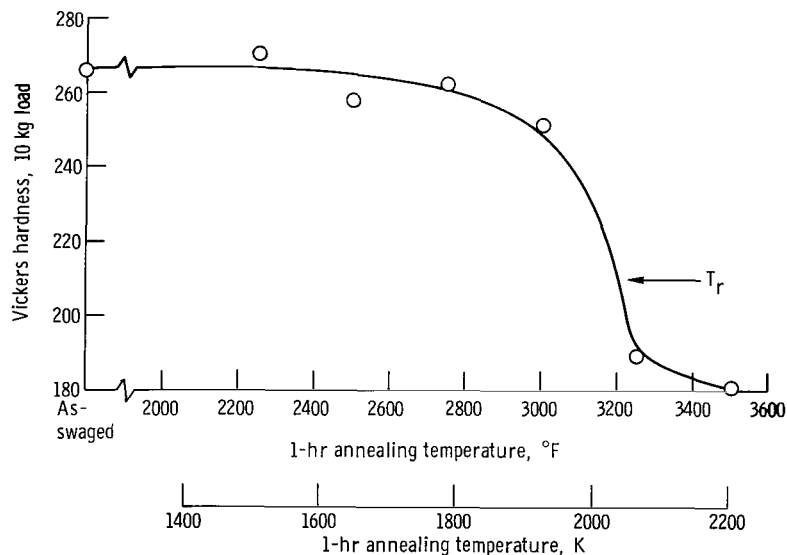


Figure 3. - Hardness as function of annealing temperature for MHC-38E-89, Mo-0.47 percent Hf-0.29 percent C.

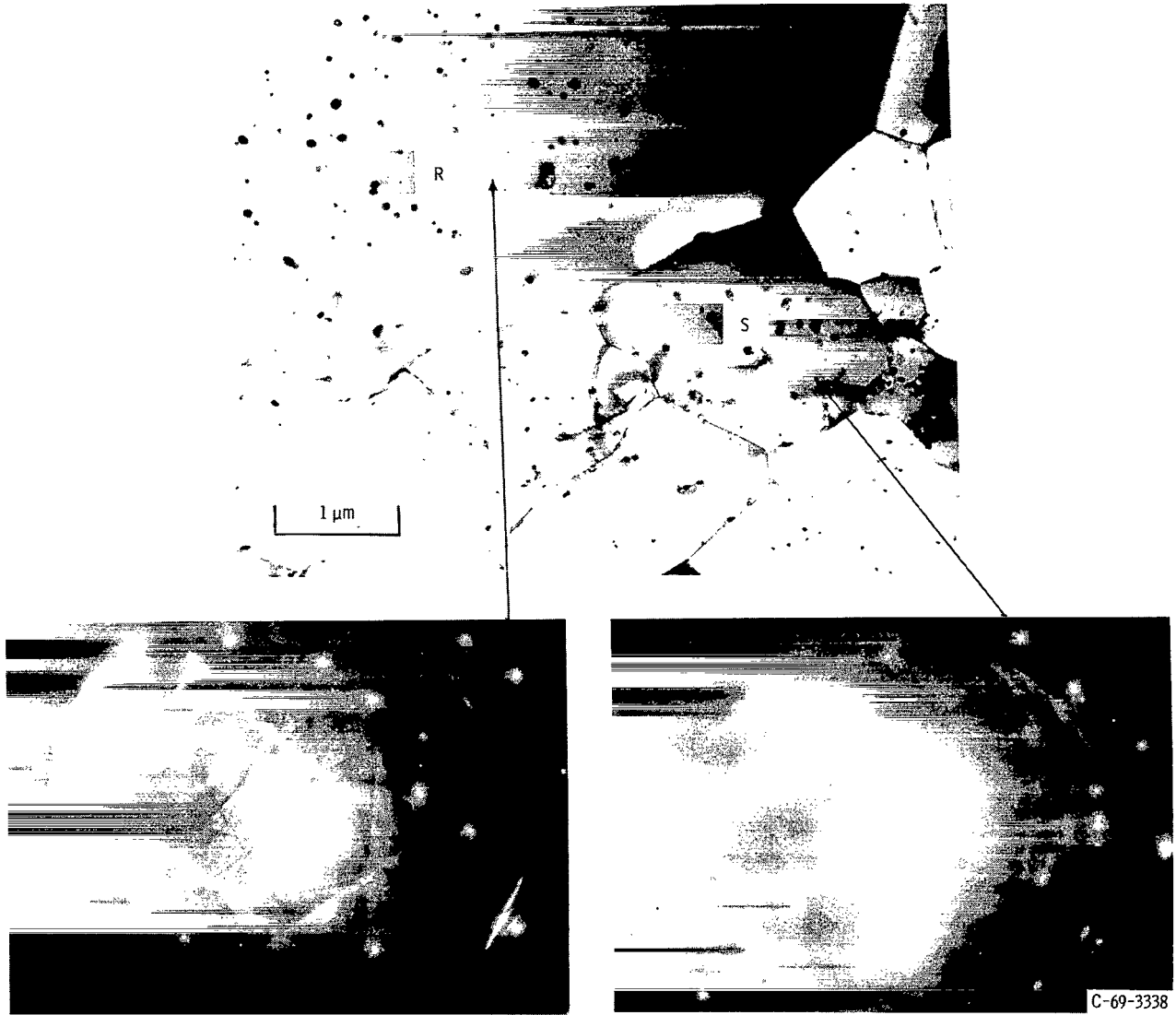


Figure 4. - Transmission electron micrograph of swaged MHC-38E-89, Mo-0.47 percent Hf-0.29 percent C after a 3000° F (1922 K) anneal for 1 hour. Micrograph includes selected area diffraction from recrystallized grain (R) and strain hardened substructure (S). Note diffuse Kikuchi lines in strain hardened region.

structural change occurred after annealing up to 2750^o F (1783 K). Specimens annealed at 3000^o F (1922 K) and higher showed signs of recrystallization as indicated by the micrograph in figure 4. The recrystallized grain R is shown growing into a subgrain structure S. The average subgrain diameter is of the order of 1 micrometer. Diffraction patterns taken from the grain R and within a subgrain are shown in the inset in figure 4. Sharp Kikuchi lines are seen in R while they are so diffuse as to be almost nonexistent in the pattern from the subgrain. This suggests that, at this stage of recrystallization, there still exist stored elastic strains within the subgrains (ref. 13).

Another important feature of the recrystallization process in MHC-38E-89 is illustrated in figure 5. This specimen was annealed for 1 hour at 3250^o F (2060 K) and again shows a recrystallized grain growing into the subgrain structure. The average particle diameter within the recrystallized grain was observed to be larger than that in the subgrains. Overall particle coarsening occurs at this temperature but it appears that the passage of the grain boundary surrounding the recrystallized grain causes an accelerated

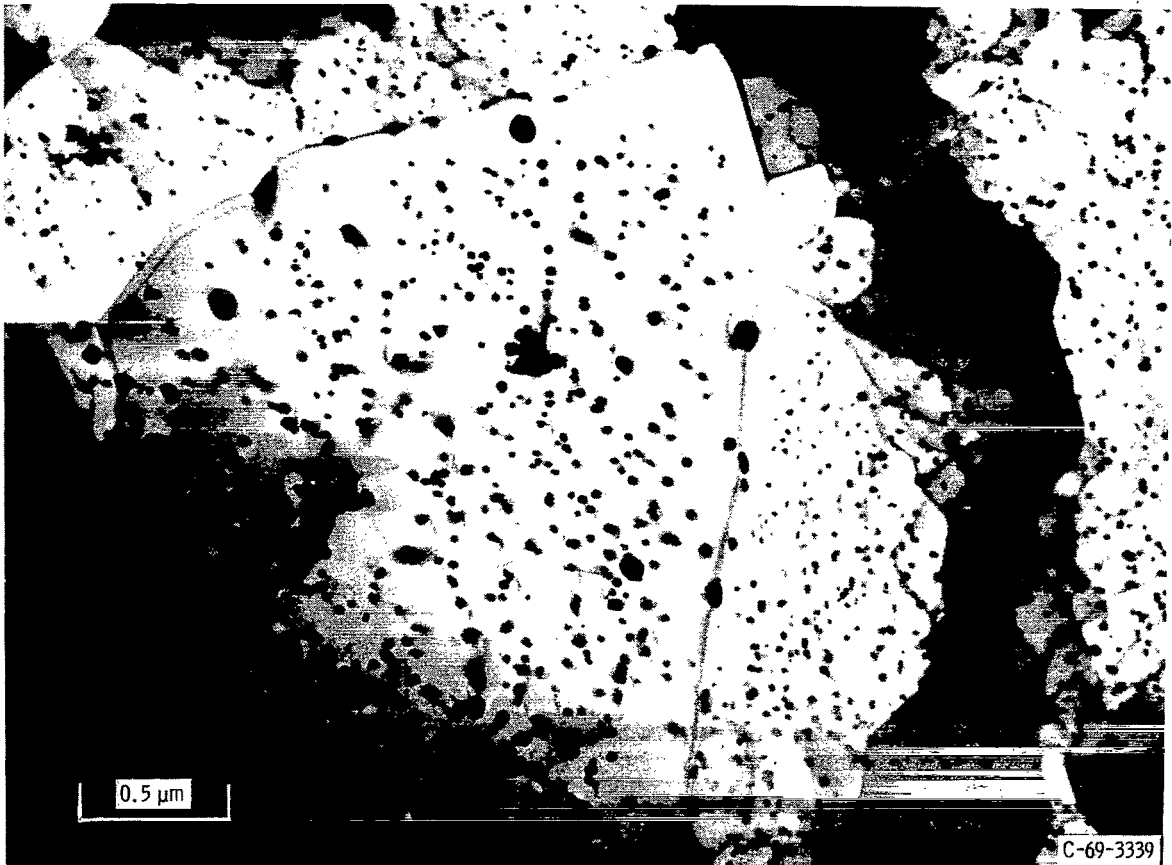


Figure 5. - Transmission electron micrograph of swaged MHC-38E-89, Mo-0.47 percent Hf-0.29 percent C, after a 1-hour anneal at 3250^o F (2060 K). Note particle growth as a result of recrystallization.

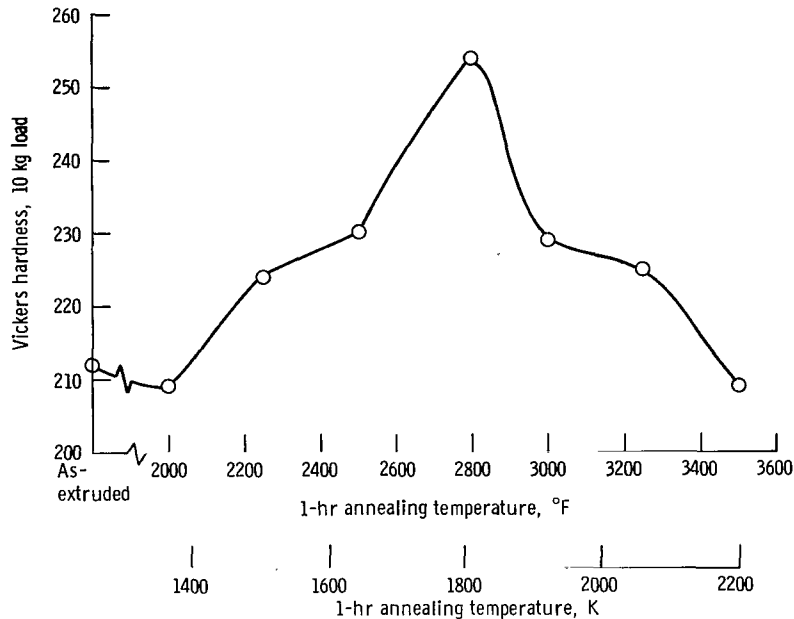


Figure 6. - Variation of hardness with annealing temperature for extruded MHC-39, Mo-0.6 percent Hf-0.5 percent C.

coarsening. Perkins (ref. 3) also observed that recrystallization causes an accelerated spheroidization of CbC platelets in the Cb-TZM alloy. The exact mechanism of this coarsening has not been investigated in detail in this study. However, it appears that the coarsening may be related to the dragging of carbide particles by the moving grain boundary as has been observed by Ashby and Centamore (ref. 14) for various oxides in copper. The carbides could be picked up by the moving boundary where they coarsen rapidly. The particles would then be left behind when they became too large to retard further migration of the boundary effectively.

The process K, which was described previously, depended on the attainment of an extruded structure which was age-hardenable. Hardness tests were performed on material from extruded Mo-0.6 percent Hf-0.5 percent (MHC-39) annealed at various temperatures for 1 hour. The results shown in figure 6 show that the extrusion does age-harden, indicating success in retaining some hafnium carbide in solid solution after the extrusion.

Tensile Properties of As-Swaged Alloys

Tensile properties obtained for material in the as-swaged condition are listed in table IV. The tensile properties were measured at room temperature and 1500⁰ to 3000⁰ F (1088 to 1922 K) although for most of the alloys only 2400⁰ F (1588 K) data were obtained for screening. Figure 7 depicts the data graphically. In figure 7(a), data for

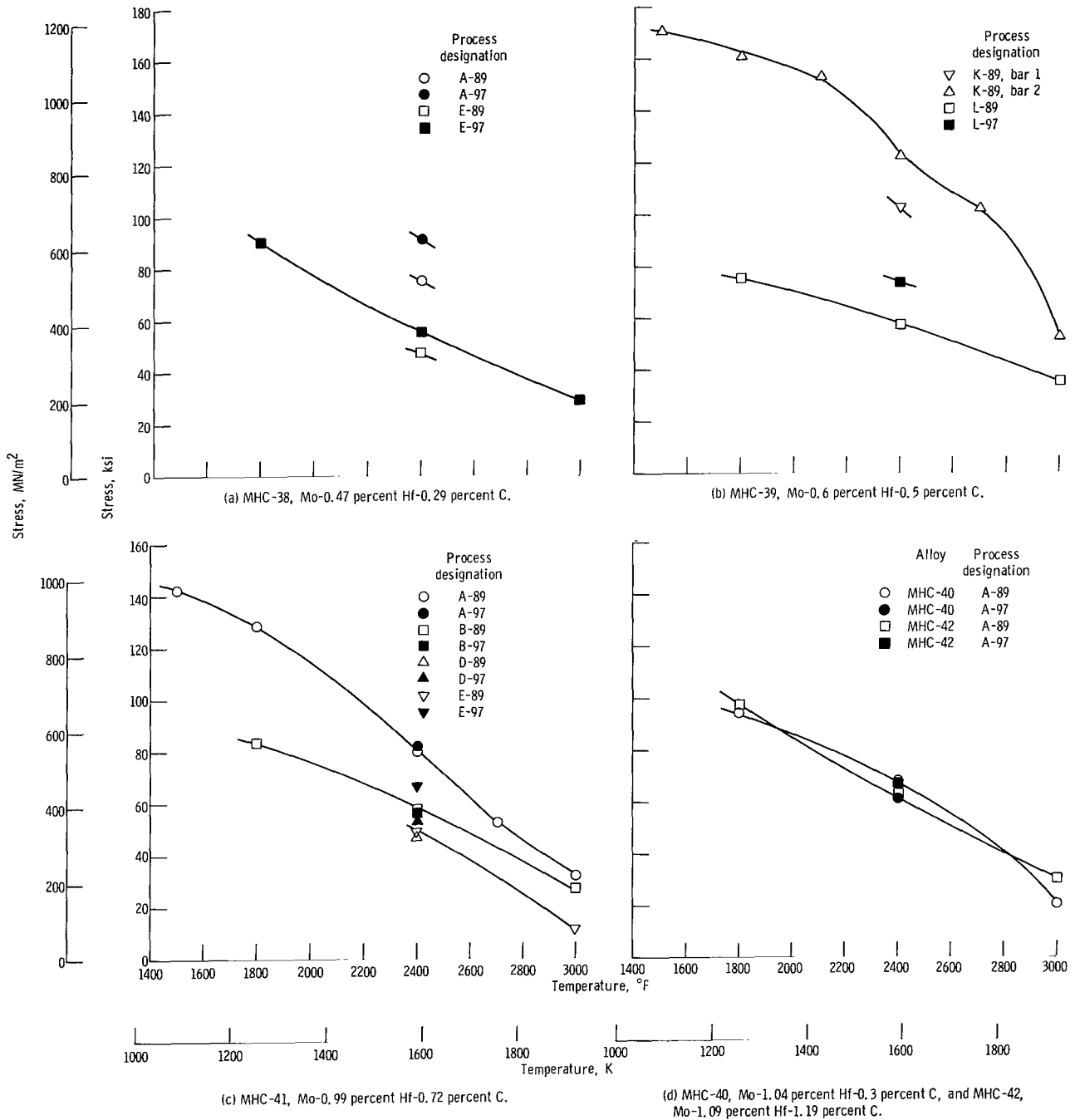


Figure 7. - Temperature dependence of ultimate tensile strength for Mo-Hf-C alloys in as-swaged condition.

MHC-38, Mo-0.47 percent Hf-0.29 percent C for the A and E processes are plotted. The tensile strengths at 2400^o F (1588 K) are higher for the A process than for the E process. For example, the ultimate tensile strength of 91.6 ksi (632 MN/m²) was obtained for MHC-38A-97 compared with 55.7 ksi (384 MN/m²) for MHC-38E-97.

Data for MHC-39, Mo-0.6 percent Hf-0.5 percent C for the K and L processes are plotted in figure 7(b). MHC-39 K-89-2 was the strongest alloy identified in this program. The fabrication schedule for this alloy consisted of extrusion from 4000^o F (2477 K) followed by swaging at 2500^o F (1644 K). The tensile strength at 2400^o F (1588 K) was 122 ksi (845 MN/m²) which is considerably higher than any other molybdenum alloy tested to date (refs. 1, 3, and 6). Another portion of this extrusion was swaged under identical conditions (MHC-39K-89-1) and had a tensile strength of 103 ksi (707 MN/m²) which is still considerably higher than any of the other alloys. The strength of MHC-39K-89-2 was investigated over the entire range of temperatures. An ultimate tensile strength of 52.6 ksi (363 MN/m²) was measured at 3000^o F (1922 K), representing a substantial increase over the range of 20 to 35 ksi (138 to 242 MN/m²) normally measured for molybdenum alloys (see ref. 6 and data for other alloys in this report).

The alloy MHC-39K-89 was swaged directly after a 4000^o F (2477 K) extrusion. The alloys designated MHC-39L-89 and MHC-39L-97 were given an aging treatment at 2800^o F (1810 K) prior to swaging. Tensile data for these two processes are also included in figure 7(b). The tensile strengths are substantially lower than that for MHC-39K-89. The possible reasons for these differences will be presented in the DISCUSSION section.

The largest number of individual processes were studied on alloy MHC-41, Mo-0.99 percent Hf-0.72 percent C. The tensile data for material from these various processes are plotted in figure 7(c). Data for processes F and G are not included for clarity. The data in figure 7(c) show the wide variation in properties which may be achieved by relatively minor alterations in the thermomechanical processing schedule. For example, the tensile strength at 2400^o F (1588 K) varies from 47.8 ksi (330 MN/m²) for the E-89 process to 81.6 ksi (536 MN/m²) for the A-97 process. Similar wide variations are seen at 3000^o F (1922 K). As in MHC-38, the strength for the E process was the lowest of those investigated. The E process consists of a 4000^o F (2477 K) solution anneal and a 2800^o F (1810 K) age prior to swaging. The tensile strength at 2400^o F in the F and G processes was higher; these processes substituted a 3800^o F (2366 K) solution anneal in place of the one at 4000^o F (2477 K).

Tensile data are given in figure 7(d) for alloys MHC-40, Mo-1.04 percent Hf-0.3 percent C and MHC-42, Mo-1.09 percent Hf-1.19 percent C in the A condition. The tensile strengths for these alloys are virtually the same over the entire temperature range.

Room-temperature elongations for all the alloys varied from 0 to 20 percent, as shown in table IV. In general, the elongation for the A process was lowest although this was improved when the total percent reduction was increased from 89 to 97 percent.

Creep-Rupture Properties of As-Swaged Alloys

Creep rupture data for the as-swaged alloys are given in table V. All the alloys were tested under the standard conditions 2400° F (1588 K) and 35 ksi (242 MN/m²). Alloys MHC-39K-89 and MHC-39L-89, Mo-0.6 percent Hf-0.5 percent C were tested at additional stresses as well. The creep data in table V indicated that, with few exceptions, the alloys with the highest short time tensile strengths did not have the highest creep strength. This is particularly evident in alloy MHC-41, Mo-0.99 percent Hf-0.72 percent C. The specimen in the A-89 condition had a tensile strength of 80 ksi (552 MN/m²) at 2400° F (1588 K) but ruptured in only 8.5 hours at 35 ksi (242 MN/m²). In contrast, the alloy in the E-89 condition had an ultimate tensile strength of only 47.8 ksi (330 MN/m²) but ruptured in 12.3 hours under the standard stress and temperature conditions.

In contrast, the alloy MHC-39K-89 was the strongest in both creep rupture and in the short time tensile properties. Figures 8 and 9 show the stress dependency of the rupture life and the minimum creep rate for MHC-39K-89 and MHC-39L-89. At 35 ksi (242 MN/m²) and 2400° F (1588 K), the alloy MHC-39K-89 ruptured in 96.1 hours which was far longer than any of the other alloys (see table V). The alloy MHC-39L-89 ruptured in 31.8 hours while MHC-39L-97 ruptured in 57.8 hours. MHC-39 in all its structural conditions was the most creep resistant alloy tested.

The stress dependence of the rupture life t_r and minimum creep rate $\dot{\epsilon}_m$ followed the standard empirical equations

$$\begin{aligned} t_r &= A\sigma^r \\ \dot{\epsilon}_m &= B\sigma^c \end{aligned} \tag{1}$$

where c and r are the stress exponents for creep and rupture, respectively. The absolute values of both c and r for MHC-39K-89 were nearly half those for MHC-39L-89, as indicated in figures 8 and 9.

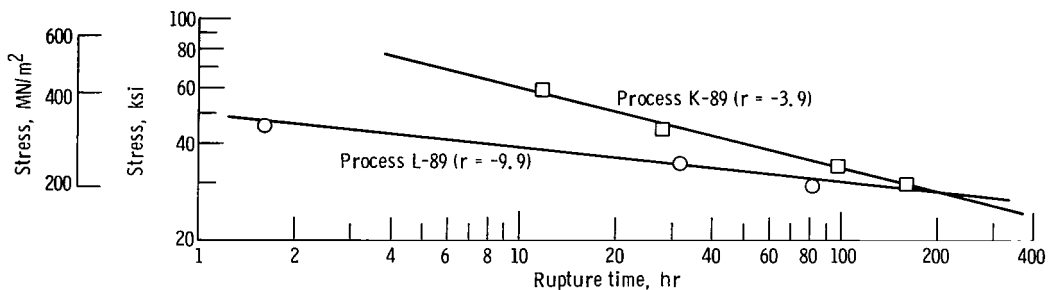


Figure 8. - Stress dependency of rupture life for alloy MHC-39, Mo-0.6 percent Hf-0.5 percent C, at 2400° F (1588 K). $t_r \sim \sigma^r$.

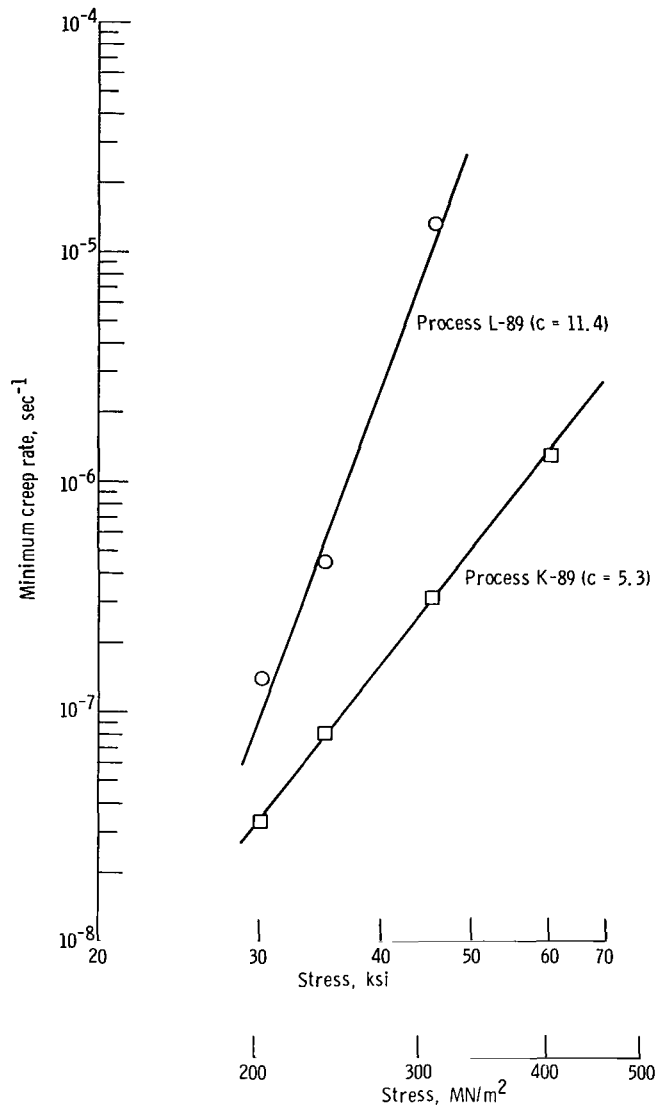


Figure 9. - Stress dependency of minimum creep rate $\dot{\epsilon}_m$ ($\sim \sigma^c$) for alloy MHC-39, Mo-0.6 percent Hf-0.5 percent C at 2400° F (1588 K).

Creep-Rupture Properties of Annealed Alloys

Specimens of MHC-38E-89 were annealed for 1 hour in the temperature range 2250° to 4000° F (1505 to 2477 K). The specimen annealed at 4000° F (2477 K) was rapidly cooled by introducing helium gas into the furnace. The specimens were then tested to rupture at 35 ksi (242 MN/m²) at 2400° F (1588 K). The results are given in table VI. Figure 10 is a plot of the rupture time as a function of annealing temperature. Annealing at temperatures up to 2750° F (1783 K) had little effect on the rupture time. At 3000° F

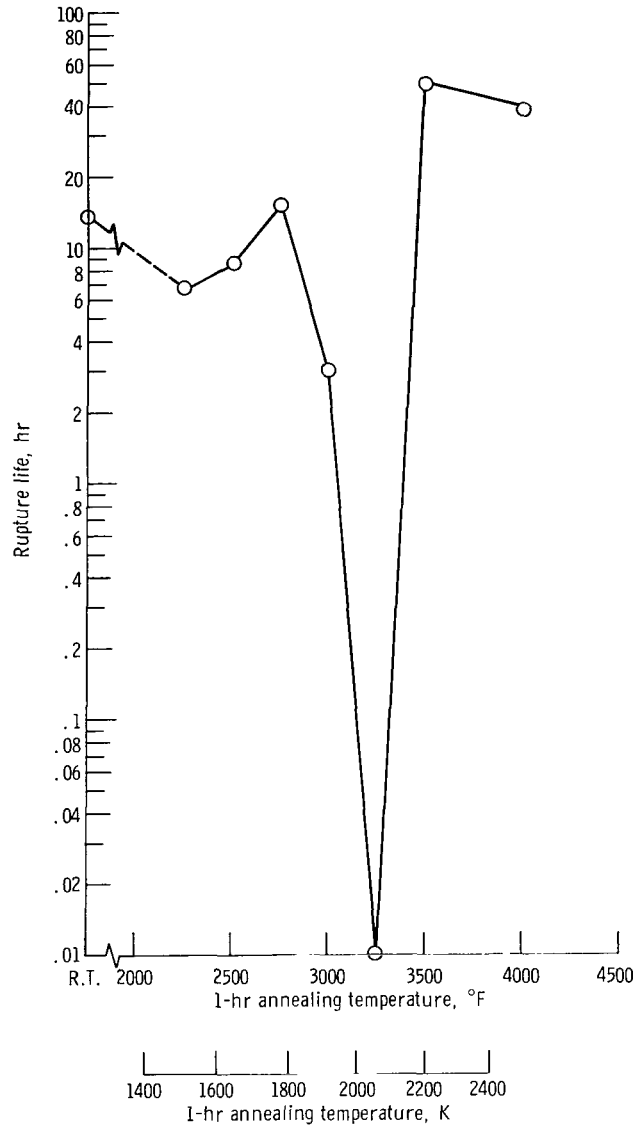
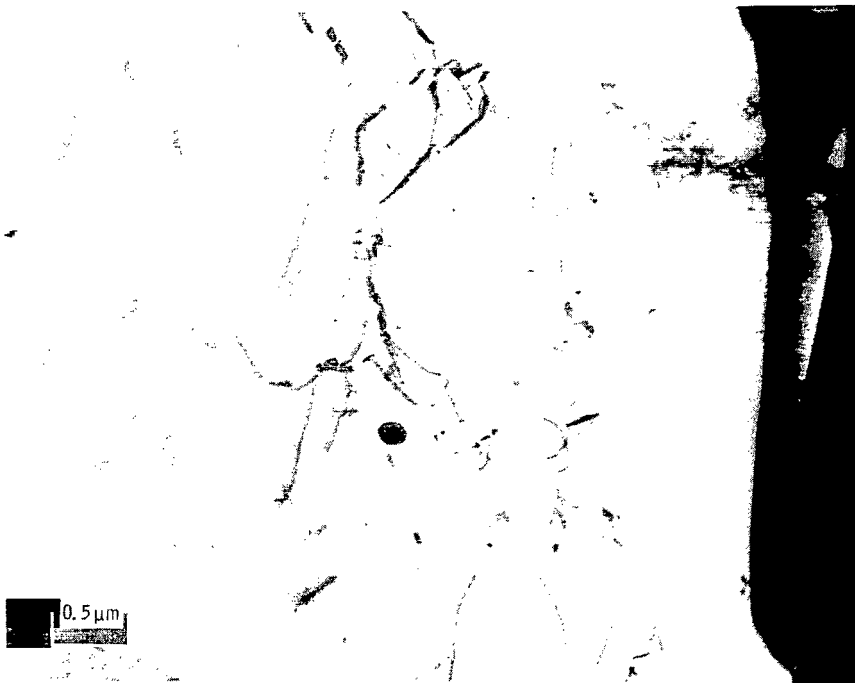


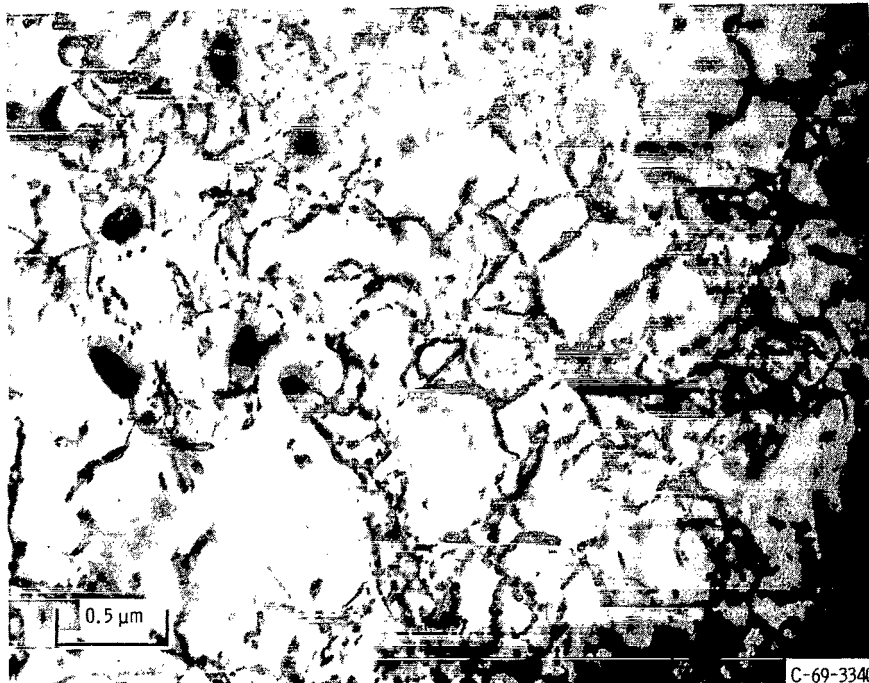
Figure 10. - Variation of rupture life at 2400° F (1588 K) and stress of 35 ksi (242 MN/m²) with annealing temperature for MHC-38E-89, Mo-0.47 percent Hf-0.29 percent C.

(1922 K), t_r decreased to 3 hours and after annealing at 3250° F (2060 K) the specimen ruptured in 0.01 hour (approx 15 sec). Annealing at temperatures of 3500° and 4000° F (2200 and 2477 K) produced a large increase in the rupture time and a decrease in the creep rate as indicated in figure 10 and table VI.

The changes in the creep strength with annealing temperature can be related to the annealing curve in figure 3. It is apparent that large changes in the rupture life do not occur until recrystallization begins, that is at 3000° F (1922 K). The rupture life was very low when recrystallization was nearly complete, that is at 3250° F (2060 K). The



(a) As solution treated.



(b) Solution treated and creep-rupture tested to failure at 35 ksi (242 MN/m²) and 2400° F (1588 K).
Note precipitation on dislocations.

Figure 11. - MHC-38E-89, Mo-0.47 percent Hf-0.29 percent C, solution treated at 4000° F (2477 K).

increase in the rupture life on annealing at the higher temperatures is believed to be the result of solutioning of the carbides during annealing. The material is then strengthened by a dynamic strengthening mechanism involving the possible simultaneous precipitation of HfC during creep (refs. 15 and 16). Figure 11 shows micrographs of the specimen annealed at 3500⁰ F (1922 K) before and after creep. Figure 11(a) can be compared with figure 5 (3250⁰ F (2060 K) anneal) and it is quite apparent that a considerable amount of carbide solutioning has taken place. After creep (fig. 11(b)), the structure consisted of a uniform dislocation array decorated by precipitates, presumably HfC. The data presented in this section illustrate the potent effect of dynamic strengthening mechanisms and these will be examined in more detail in the DISCUSSION section.

Properties of Hydrostatically Extruded Molybdenum-TZC Alloy

Figure 12 shows the room-temperature hardness of hydrostatically extruded Mo-TZC after annealing for 1 hour at the indicated temperatures. Included in figure 12 are data for the same alloy which had been solution annealed without extrusion. Some age hardening was noted in each set of specimens but the hardening was greater in the extruded

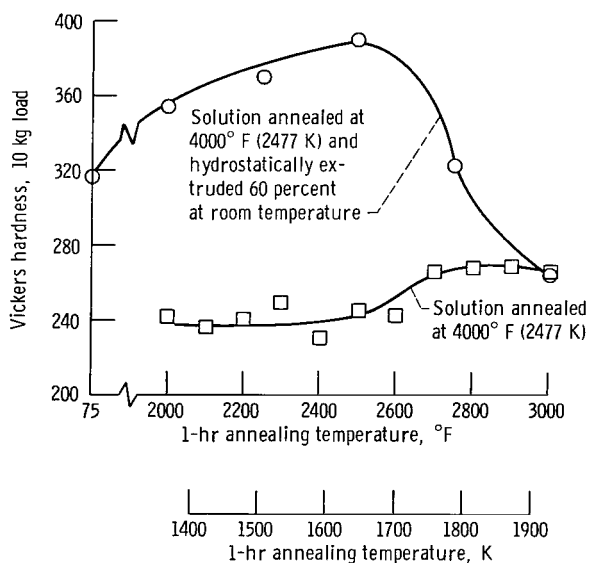


Figure 12. - Variation of hardness with annealing temperature for molybdenum-TZC alloy.

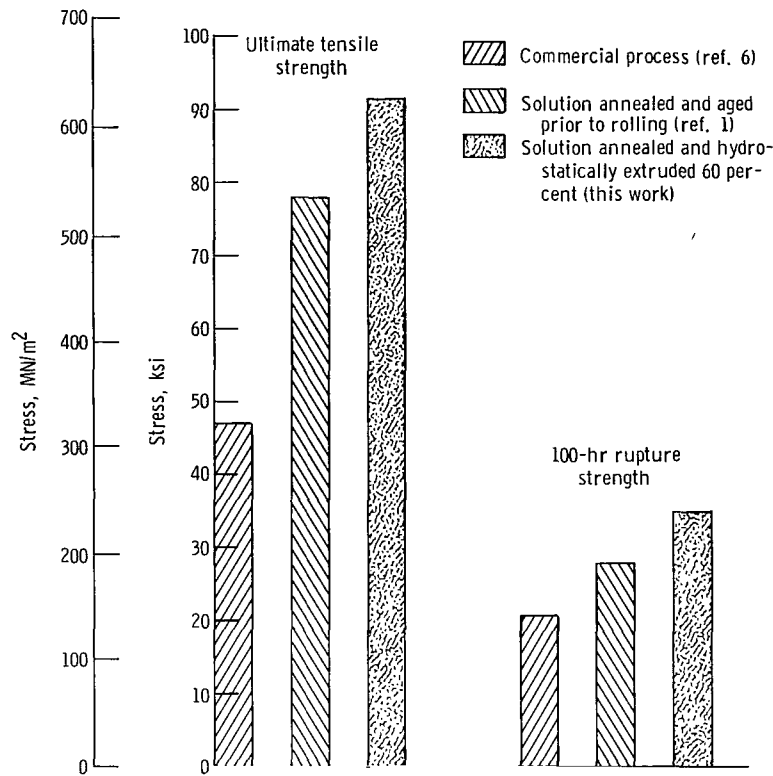


Figure 13. - Ultimate tensile strength and 100-hour stress rupture strength at 2400° F (1588 K) for wrought Mo-TZC after three different thermomechanical treatments.

material. The solution annealed material began to harden at approximately 2700° F (1755 K), while the extruded material showed a large hardness increase as low as 2000° F (1366 K). It appears that the substructure introduced during extrusion is acting to increase the rate of precipitation. This probably occurs by the dislocations acting as carbide nucleation sites. The decrease in hardness that occurs above 2500° F (1644 K) is caused by recrystallization which was observed metallographically.

One of the specimens was tested in tension at 2400° F (1588 K), while the other was tested in creep rupture under the standard conditions used in the previous tests. Figure 13 compares the ultimate tensile strength at 2400° F (1588 K) and the approximate stress for 100-hour rupture¹ for Mo-TZC after three different thermomechanical treatments. The process of solution annealing and aging prior to rolling represents the optimum process found by Semchyshen et al. (ref. 1) for this alloy. In both cases, the strength of hydrostatically extruded Mo-TZC is superior to the other processes. Electron

¹The hydrostatically extruded Mo-TZC specimen ruptured at 106 hours and thus the 100-hour rupture stress was used as 35 ksi (242 MN/m²).

microscope evidence was found for simultaneous carbide precipitation during creep; this is discussed later.

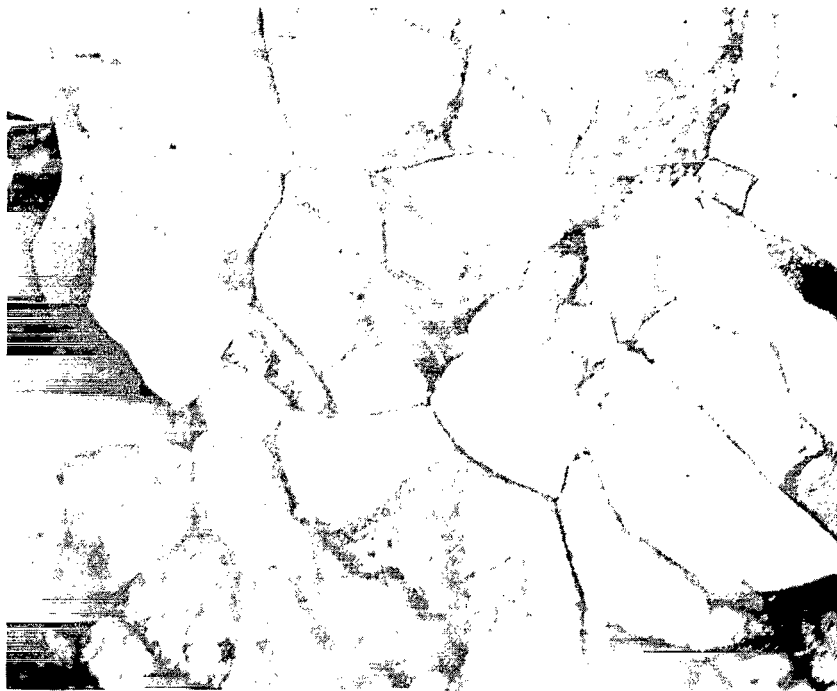
Metallography of As-Swaged Alloys

Throughout this program, the microstructure of the alloys was studied using transmission electron microscopy. In addition to the alloys prepared for this work, specimens for microscopy were also taken from the Mo-Hf-C alloys studied by this author in reference 6. The general purpose of these studies was to correlate the microstructures with the various processing steps and the measured mechanical properties. These latter correlations are the main subject of the DISCUSSION section.

Figure 14 shows a micrograph of unalloyed molybdenum in the as-swaged condition. This arc-cast molybdenum was obtained commercially. Subgrains with an average diameter of approximately 1.25 micrometers are apparent in this transverse section. Few dislocations were observed within the subgrains, which were equiaxed and uniform in size. Figure 15 shows the changes in substructure as hafnium and carbon are added. The alloys in figure 15 are in the A-89 condition and their mechanical property data were



Figure 14. - Transmission electron micrograph of commercial swaged molybdenum rod. Transverse section.

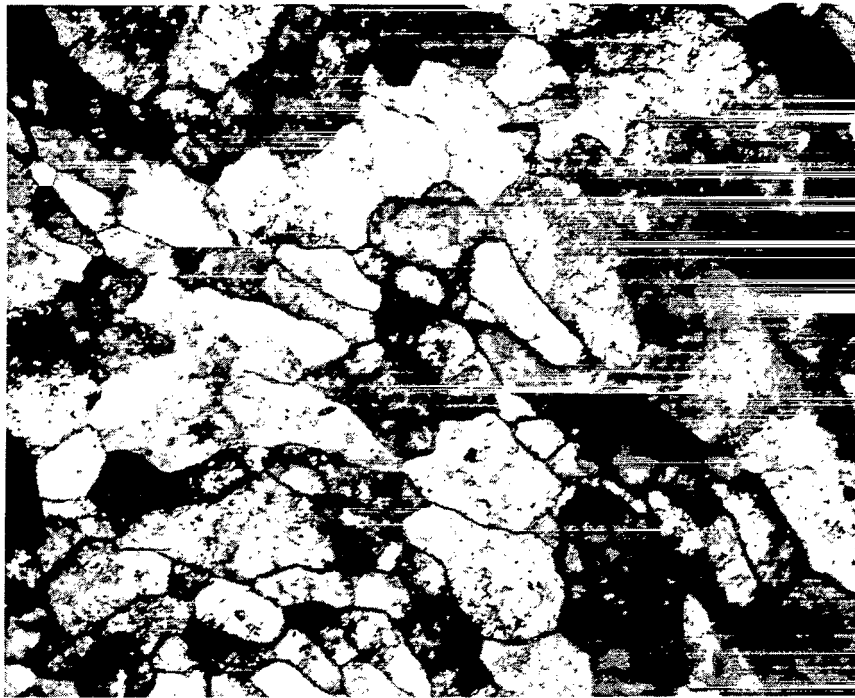


(a) MHC-21A-89, Mo-0.18 percent Hf-0.42 percent C.

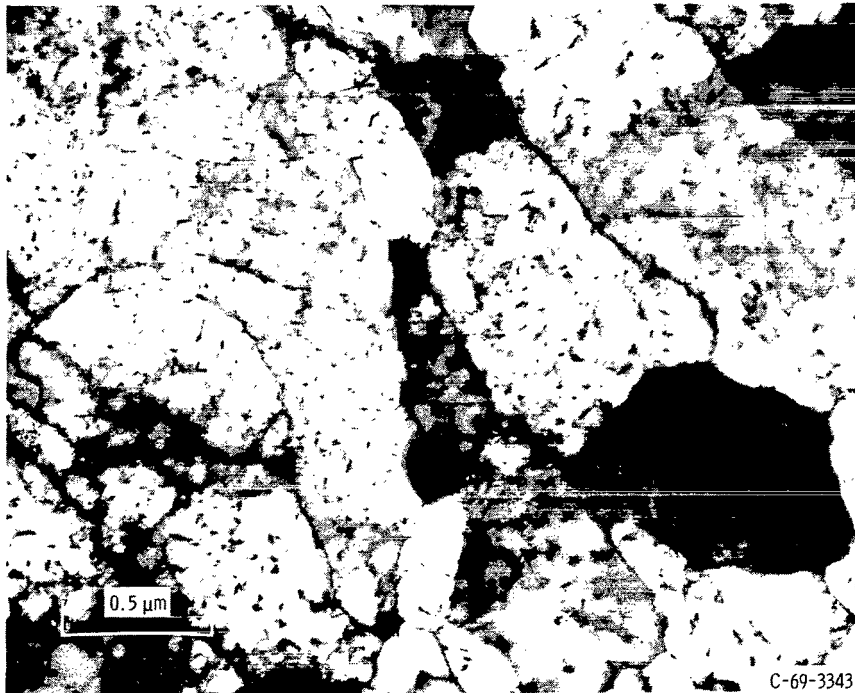


(b) MHC-27A-89, Mo-0.98 percent Hf-1.11 percent C.

Figure 15. - Transmission electron micrographs of two typical Mo-Hf-C alloys studied in reference 6. Transverse section.



(a) Process A-89.

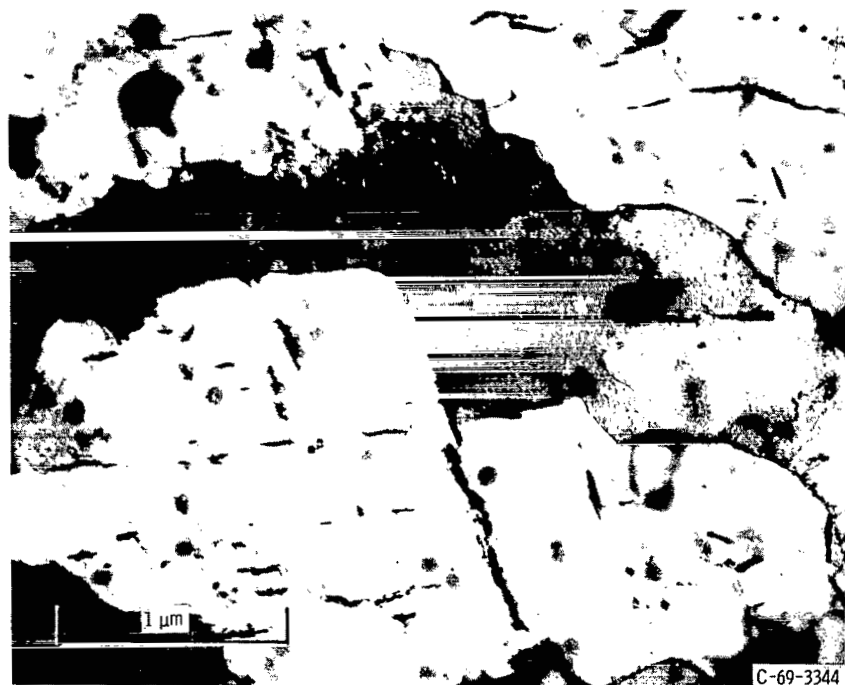


(b) Process E-89.

Figure 16. - Comparison of microstructures for swaged alloy MHC-38, Mo-0.47 percent Hf-0.29 percent C with two different processing schedules.



(a) Process A-89.



(b) Process E-89.

Figure 17. - Comparison of microstructure for swaged alloy MHC-41, Mo-0, 99 percent Hf-0, 72 percent C, with two different processing schedules.

reported in reference 6. The main effects of alloying were (1) a refinement of the subgrain size, (2) an increase in the dislocation density within the subgrains, and (3) a tendency for the subgrains to become less equiaxed. An attempt was made to measure the misorientation between adjacent cells using the Kikuchi line shift (ref. 13). However, the Kikuchi lines were extremely diffuse, apparently due to the stored elastic strains (see fig. 4).

Figure 16 shows a comparison of the substructure of the A and E processed material for MHC-38, Mo-0.47 percent Hf-0.29 percent C. The subgrain size was smaller for the material made by the A process than for that made by the E process (0.44 μm compared with 0.80 μm). The structure of the material from the E process, however, contained numerous fine platelets, presumably of HfC, which were formed by the aging treatment given this alloy prior to swaging. Figure 17 shows a similar comparison of the A and E processes for MHC-41, Mo-0.99 percent Hf-0.72 percent C. The platelet size in MHC-41E-89 (fig. 17) is greater than that for MHC-38E-89 (fig. 16), while the subgrain diameter is smaller (0.54 μm for MHC-41E-89). The microstructure of MHC-41A-89 (fig. 17(a)) shows a dense dislocation structure within the cells, although the visible carbides are relatively large and widely spaced.

Table VII lists the measured average subgrain diameters for all the alloys investigated in this work and in reference 6. Also included in table VII are the room-temperature and 2400⁰ F (1588 K) yield strengths which are discussed later in this report. The subgrain sizes ranged from 0.34 to 1.20 micrometers. There was no apparent correlation of subgrain size with composition for a constant processing treatment. The subgrain sizes were generally observed to decrease as the amount of reduction during swaging increased.

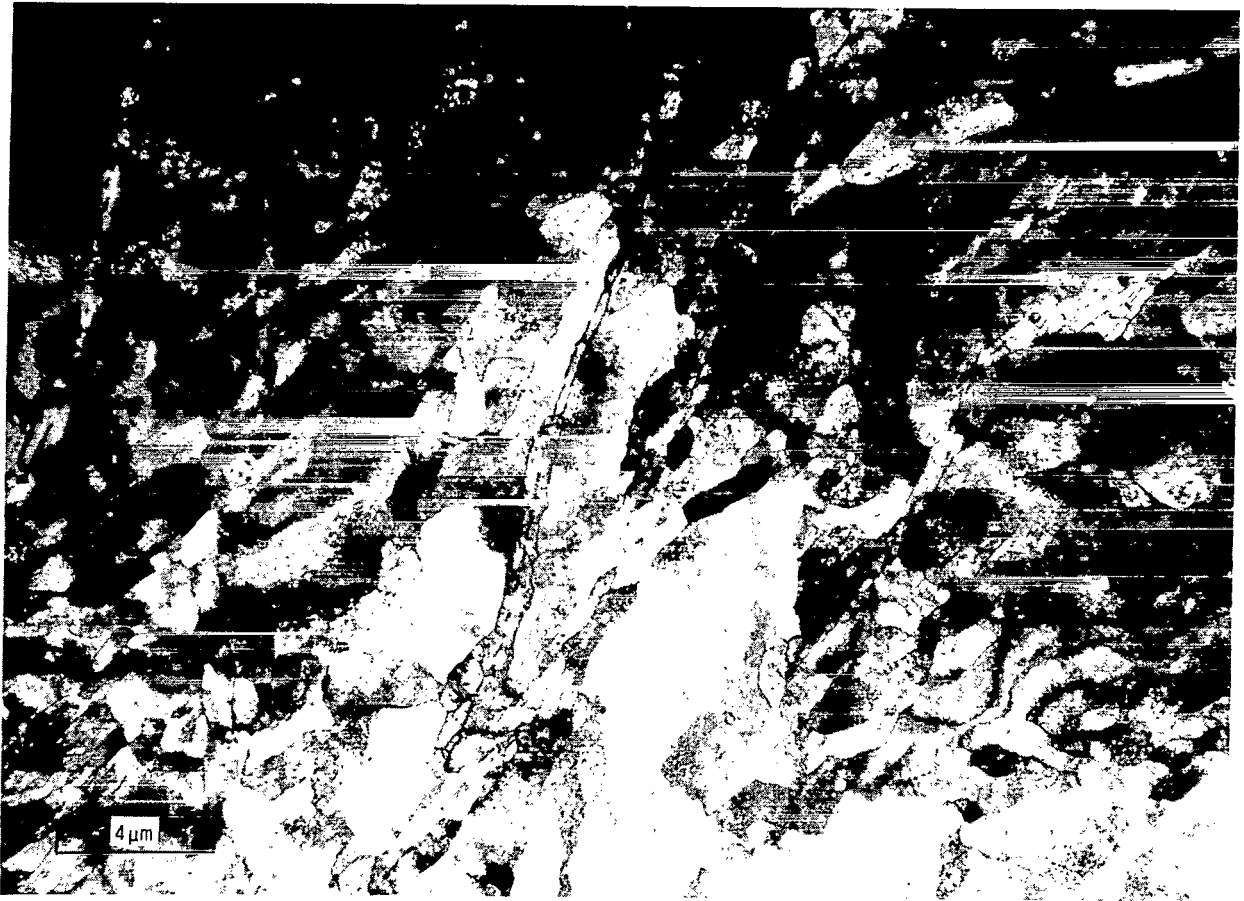
Metallography of MHC-39

A considerable amount of electron microscopy was performed on the alloy MHC-39, Mo-0.6 percent Hf-0.5 percent C. Emphasis was placed on this alloy because of its high strength compared with the other alloys. Figure 18 is a micrograph of MHC-39 after the 4000⁰ F (2477 K) extrusion. Some coarse, widely spaced carbide platelets are evident as well as a considerable amount of precipitation on the subgrain boundaries. However, the structure does correspond to a typical "solution annealed" structure in carbide strengthened molybdenum alloys. This structure is age-hardenable as indicated in figure 6.

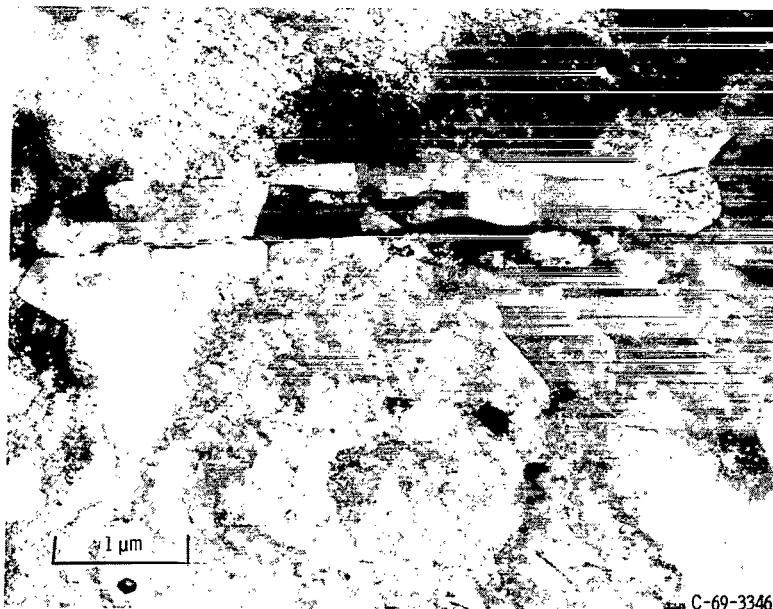


Figure 18. - Transmission electron micrograph of extruded MHC-39, Mo-0.6 percent Hf-0.5 percent C. Transverse section.

The microstructure of MHC-39K-89 in the as-swaged condition is shown in figure 19. The microstructure has some important differences compared with the other alloys. First, the average subgrain size is of the order of 1.2 micrometers, more typical of unalloyed molybdenum than the Mo-Hf-C alloys. However, the subgrain boundaries are quite diffuse, a factor which adds an uncertainty to this value. Second, the dislocation density within the cells is considerably higher than in the other alloys. Finally, a significant feature of the microstructure of this alloy is the presence of bands of slightly elongated subgrains. The bands are magnified in figure 19(b). Whereas the misorientation between subgrains within the body of the structure is small, misorientations of approximately 7° rotated about $\langle 111 \rangle$ were observed within the bands. Except for an occasional coarse particle (see fig. 19(b)), no carbides could be resolved.



(a) X6000.



(b) X20 000.

Figure 19. - Representative transmission electron micrographs of swaged MHC-39K-89, Mo-0.6 percent Hf-0.5 percent C.



Figure 20. - Transmission electron micrograph of swaged MHC-39K-89-1, Mo-0.6 percent Hf-0.5 percent C, creep tested at 2400° F (1588 K) and 35 ksi (242 MN/m²).

The microstructure of MHC-39K-89 after creep at 2400° F (1588 K) is shown in figure 20. The creep straining has removed most of the dislocations within the subgrains. However, there now exists a fine dispersion of HfC particles, many of which are 100 Å or less in diameter. These particles were either present as smaller particles prior to creep or were precipitated during creep. The latter could account for the high strength of this alloy, a point which is discussed later.

The alloys MHC-39L-89 and MHC-39L-97 were also examined extensively. The thermomechanical process for these alloys differed from that of MHC-39K-89 in that a 2800° F (1810 K) anneal was given to the extrusion prior to swaging. Figure 21 shows a representative high-magnification photograph of MHC-39L-97. The subgrain structures

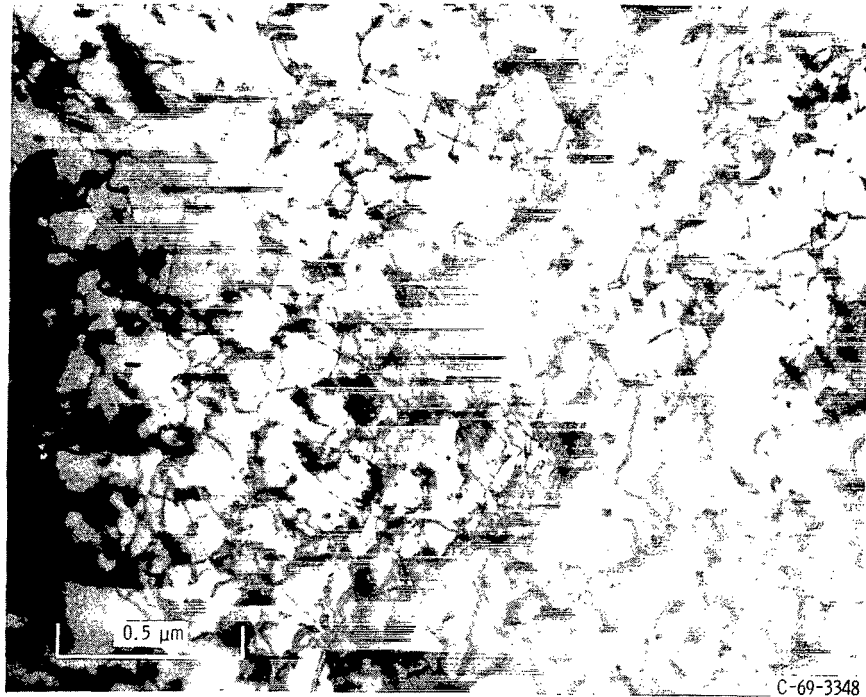
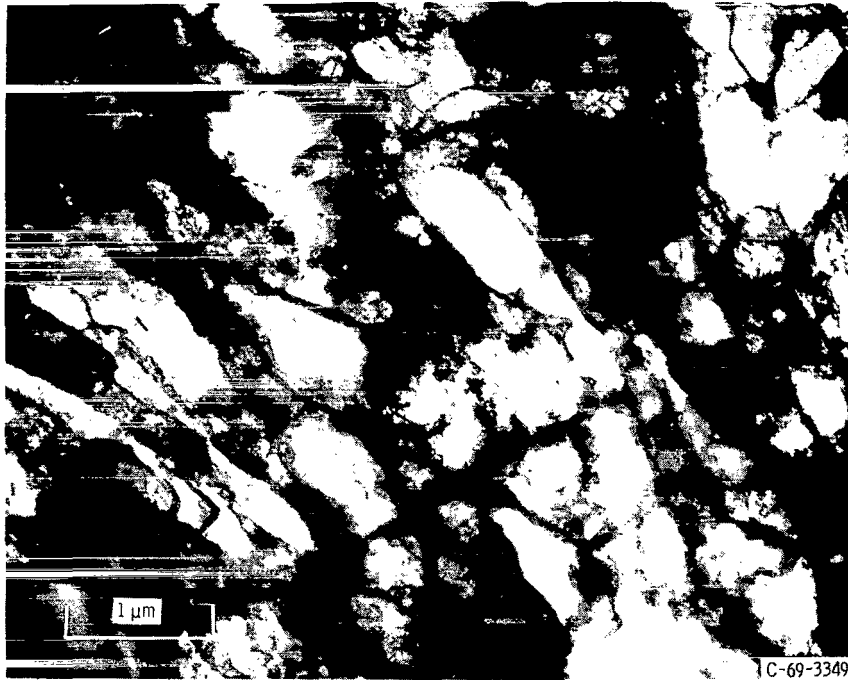


Figure 21. - Microstructure of swaged MHC-39L-97, Mo-0.6 percent Hf-0.5 percent C. Transverse section.

of the alloys after these L processes were similar to those of the other alloys with the exception of the more uniform distribution of carbides shown in figure 21. The carbides in this alloy were less than 500 Å in diameter.

Metallography of Hydrostatically Extruded Molybdenum-TZC

Some limited studies were conducted to define the microstructure of the hydrostatically extruded Mo-TZC. A low-magnification micrograph of the as-extruded structure is shown in figure 22. The structure consists of subgrains as in the as-swaged alloys, but they are considerably more diffuse than in the alloys which were swaged at higher temperatures. The structure of hydrostatically extruded Mo-TZC is typical of body-centered cubic metals, heavily deformed at low temperature (ref. 17). The higher magnification photograph in figure 22(b) shows the interior of one of the subgrains and no carbide particles are apparent. However, after creep of this alloy, a structure similar to that of MHC-39K-89 was observed with a fine distribution of carbides which evidently precipitated during creep.



(a) X20 000.

Figure 22. - Transmission electron micrographs of hydrostatically extruded Mo-TZC alloy. Transverse section. Structure shown here is typical of heavily cold worked body-centered cubic metals and alloys.



(b) X75 000; note absence of carbide particles.

Figure 22. - Concluded.

DISCUSSION

In previous sections, the mechanical properties of a series of Mo-Hf-C alloys have been shown to be strongly related to the type of thermomechanical processing schedule used. The variables involved in the thermomechanical processing of molybdenum alloys could be better understood if the mechanical properties could be related to the measured microstructural features. This is the theme of this section. It is hoped that this discussion will allow a clearer definition of the relevant strengthening mechanisms and perhaps aid in designing a processing schedule for the alloys which would focus on refining the important microstructural features of a given alloy.

The general microstructure of most of the alloys is dominated by a network of irregularly shaped subgrains. Superimposed on this subgrain structure is an array of hafnium carbide particles. Both the size of the subgrains and the spacing between the particles is related to the alloy composition as well as the processing schedule. In some alloys, the carbides are either nearly spherical and uniformly distributed or aligned in the swaging direction. In other alloys, the carbides were present as platelets inherited from a preswaging, aging treatment. In succeeding sections the variation of mechanical properties with the type of processing schedule will be correlated with these microstructural characteristics.

Mechanical Properties of Overaged Alloys

Wilcox (ref. 18) has suggested that the yield stress σ_y of a wrought carbide strengthened molybdenum alloy could be related to structure by the Hall-Petch equation

$$\sigma_y = \sigma_0 + kd^{-1/2} \quad (2)$$

where d is the subgrain size and σ_0 and k are constants. The constant σ_0 is presumably related to the direct strengthening effect of the particles; the value of k is proportional to the barrier strength of the subgrain boundaries. The yield strengths for several alloys have been correlated using equation (2) in figures 23 and 24. The yield strength at room temperature and 2400° F (1588 K) is plotted in figure 23 for the many processing variations on a single composition MHC-41, Mo-0.99 percent Hf-0.72 percent C. The data at both temperatures roughly fit equation (2) and the value of k at 2400° F (1588 K) is approximately one-fourth that at room temperature. Data for the A processing condition for various hafnium and carbon contents are similarly plotted in figure 24. The trend of increasing yield strength with smaller subgrain size remains.

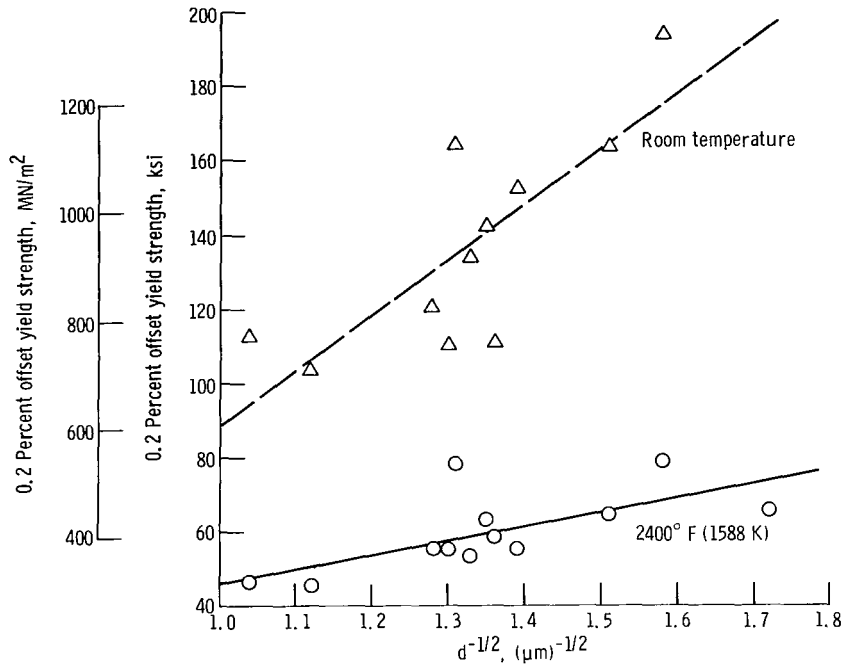


Figure 23. - Variation of yield strength with subgrain diameter for MHC-41, Mo-0.99 percent Hf-0.72 percent C, in various processed conditions.

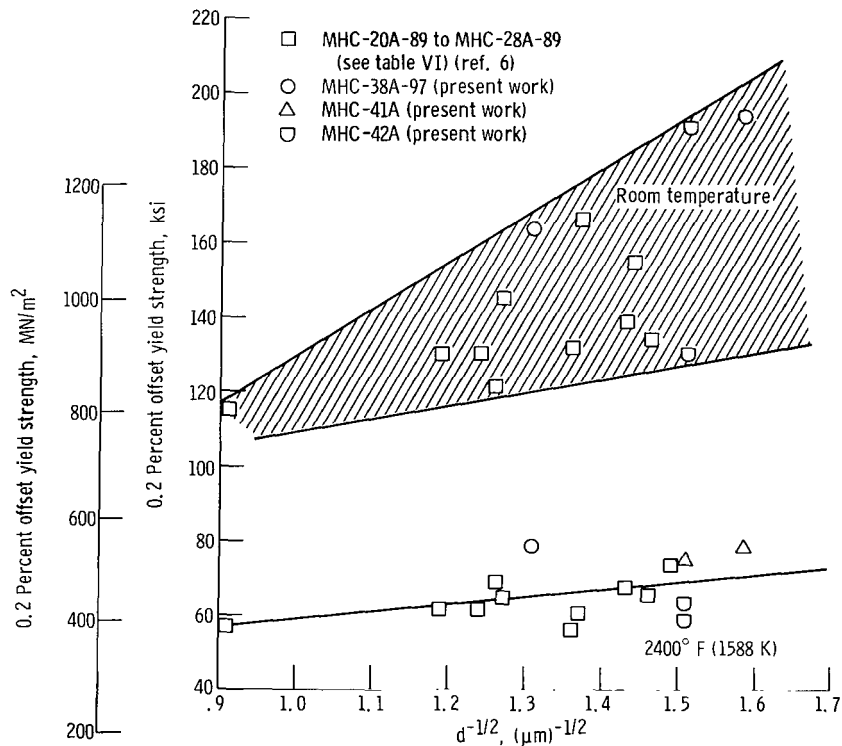


Figure 24. - Variation of yield strength with subgrain size for Mo-Hf-C alloys in the A processing condition.

The variation of σ_y with d represents a hardening effect of the subgrain boundaries acting as barriers to dislocation motion (refs. 17 and 19). It is clear that the strength of the barriers, as indicated by the value of k , decreases with increasing temperature. Electron microscopy observations indicated that the subboundaries became sharper upon heating at 2400° F (1588 K) suggesting that the decrease in k may result from this change in the boundary structure.

The value of σ_0 is taken to be constant in this analysis. However, if it is indeed related to the particle size and distribution (ref. 19), the value of σ_0 will vary from alloy to alloy and would contribute to the scatter in figure 24. Attempts were made to use the particle size and spacing to alleviate this scatter, but these were unsuccessful. It is probable that the strength of the wrought alloys in figures 23 and 24 is comprised both of a term related to the carbide distribution and to a barrier hardening effect of the subgrain boundaries. More experiments on alloys with the identical particle size and spacing but with varying subgrain size will have to be performed in order to make a clearer separation between the two effects.

Data for most of the other alloys and processes fell within the scatter in figures 23 and 24. There were important exceptions, however. The strength of MHC-39K-89 at 2400° F (1588 K) was 122 ksi (845 MN/m²) in spite of its relatively large subgrain size of 1.2 micrometers (see table VII). Clearly, additional factors control the strengthening in this alloy. It should be noted that the alloys which did fit generally into the trend suggested by equation (2) consisted of an overaged particle distribution within a strain hardened matrix. For our purposes, these will be designated overaged alloys and they are characterized by having a strength which roughly follows a form of equation (2). Alloys other than these will be designated as strain aged and will be shown to include MHC-39K-89 and hydrostatically extruded Mo-TZC. Possible sources for their strength will be suggested in a later section.

It was indicated in an earlier section that those alloys with high tensile strength at 2400° F (1588 K) did not necessarily have correspondingly high creep strength. It seems clear then that the barrier strengthening contribution suggested by figures 23 and 24 would not be effective during creep. The differences in the creep strength among these alloys might be expected to depend more on the HfC distribution. Good correlations of mechanical properties with particle size and spacing depend on the unambiguous definition of particle size and spacing. Such definitions are only available for spherical particles (ref. 9). In only a few of the alloys studied in this program could this condition be approximated. The particle sizes and spacings were thus calculated for these alloys.

Figure 25 is a plot of the minimum creep rate $\dot{\epsilon}_m$ against this mean interparticle spacing L . This plot was drawn only for those alloys where a meaningful value of L could be measured. A reasonably good fit is seen to result where the minimum creep rate is proportional to $L^{2.9}$. No simple relation could be found between the value of L

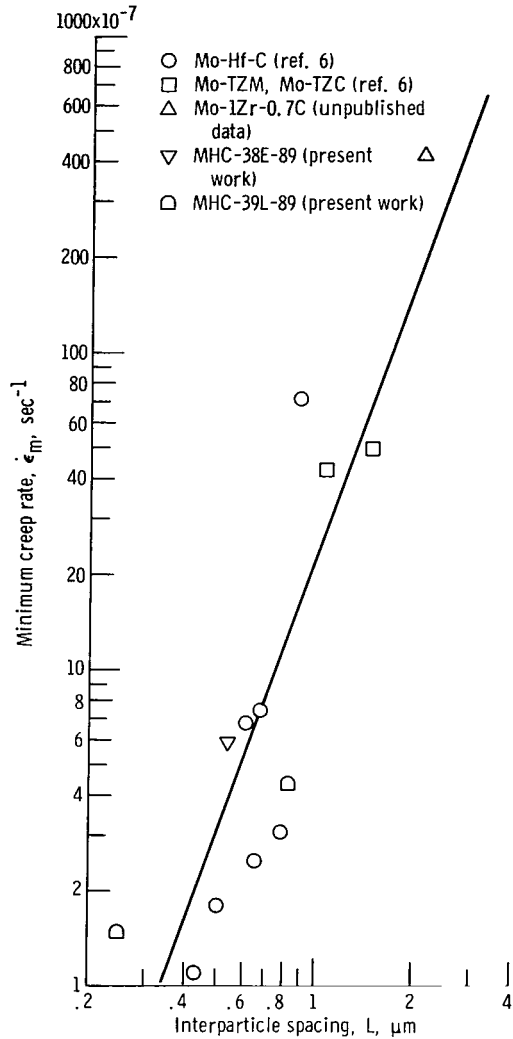


Figure 25. - Variation of minimum creep rate $\dot{\epsilon}_m$ ($\sim L^{2.9}$) at 2400° F (1588 K) and 35 ksi (242 MN/m²) with interparticle spacing L.

and the subgrain size. It can thus be concluded that the spacing between the particles primarily controls the creep strength, at least for these overaged alloys.

Mechanical Properties of Strain Aged Alloys

The preceding considerations suggest that, in the overaged alloys, the cell size and particle spacing controlled short time tensile strength, while the particle spacing alone controlled the creep properties at 2400° F (1588 K). However, the best combination of properties resulted in alloys MHC-39K-89 and hydrostatically extruded Mo-TZC. Neither

of these alloys had a microstructure similar to that for the overaged alloys. The microstructures of these alloys were virtually free of resolvable particles (see figs. 19 and 22) and it was observed that precipitation apparently occurred during creep deformation (see fig. 20). It was shown in figure 10 that a large increase in the creep strength of MHC-38E-89, Mo-0.47 percent Hf-0.29 percent C, could be achieved by annealing under conditions where precipitation could be caused to occur during creep. It can be shown that this condition may also exist in the strain aged wrought alloys, MHC-39K-89 and hydrostatically extruded TZC. Figure 26 shows a plot of the instantaneous creep rate $\dot{\epsilon}$ against time t for two annealing conditions on MHC-38E-89. For annealing temperatures below 3250^o F (2060 K), $\dot{\epsilon}$ decreased smoothly with time during transient creep and eventually reached a minimum. The $\dot{\epsilon}$ against t curve for specimens annealed at 3500^o and 4000^o F (1922 and 2477 K) contained a number of discontinuities, as shown in figure 26. Such discontinuities are peculiar to many materials where it is known that precipitation occurs during creep (ref. 15). In figure 27, a similar plot is shown for hydrostatically extruded Mo-TZC. Here the discontinuities are even more prevalent. The last example in figure 28 shows $\dot{\epsilon}$ against t plots for MHC-39K-89 and MHC-39L-89. The curve for MHC-39L-89 is smooth (an overaged alloy), while that for MHC-39K-89 showed a discontinuity after approximately 10 hours. It appears then that the creep strength of the strain aged alloys is affected by a "dynamic strengthening" process

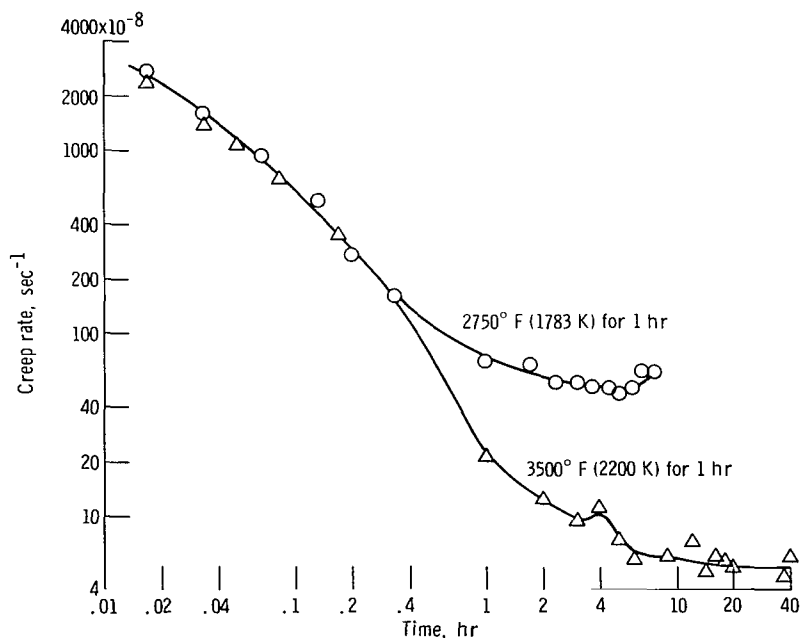


Figure 26. - Creep-rate - time plot for MHC-38E-89, Mo-0.47 percent Hf-0.29 percent C. Materials were annealed at indicated temperatures and tested at 2400^o F (1588 K) and 35 ksi (242 MN/m²).

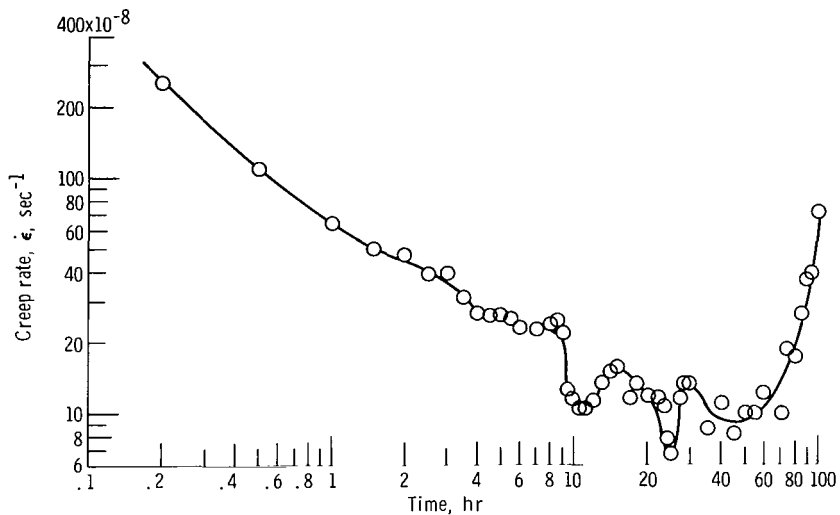


Figure 27. - Creep-rate - time plot for hydrostatically extruded Mo-TZC tested at 2400° F (1588 K) and 35 ksi (242 MN/m²).

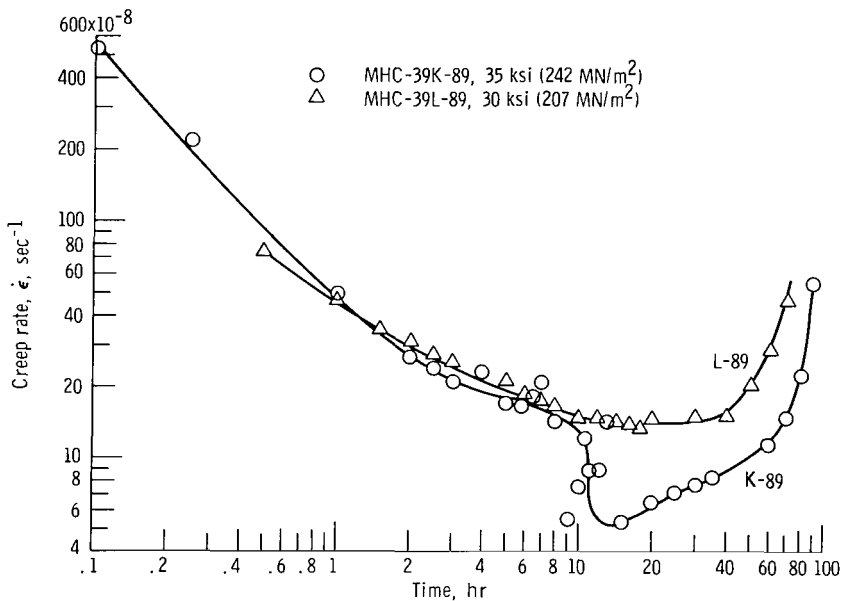


Figure 28. - Creep-rate - time plots for MHC-39, Mo-0.6 percent Hf-0.5 percent C at 2400° F (1588 K).

(ref. 18) involving the precipitation of carbides during creep, as has been indicated previously.

Another apparent difference in the mechanical behavior of the overaged and strain aged alloys is afforded by the stress dependence of the minimum creep rate. In figure 9, it was shown that, for MHC-39K-89, the value of c was 5.3, while it had a value of 11.4 for MHC-39L-89. The theoretical significance of these differences in value remains to be determined, however.

One other possibility for the high strength of MHC-39K-89 is that dynamic strengthening occurs during swaging producing a structure which has the observed high strength. This is particularly attractive in light of the lack of dynamic strengthening characteristics seen in the tensile data as shown in figure 7(b). Dynamic strengthening is usually accompanied by serrated stress-strain curves and a peak in the flow stress-strain curves due to an anomalously high work hardening rate (ref. 20). No such behavior was observed for this alloy. It is possible that precipitation occurred during swaging at 2500^o F (1644 K) resulting in a rapid rate of work hardening and the formation of an ultrafine distribution of hafnium carbide particles. The micrographs in figure 19 do not show these particles clearly, but the particles in the creep specimen in figure 20 may have grown from smaller particles. We postulate that the strength of MHC-39K-89 results from both processes: dynamic strengthening during deformation which leads to the observed high dislocation density and apparent very fine particle spacing from precipitation during creep leading to the observed discontinuities in the $\dot{\epsilon}$ against t curve (fig. 28).

Comparison with Other Studies on Thermomechanical

Processing of Molybdenum Alloys

There have been a number of investigations of the thermomechanical processing of carbide strengthened molybdenum alloys. Primary concern has been given to alloys in the Mo-Ti-Zr-C (Mo-TZC, refs. 1 and 2) and the Mo-Cb-Ti-Zr-C (Mo-Cb-TZM, ref. 3) alloy systems. The optimum processing condition reported for these alloys produces what has been designated in this report as an overaged alloy. This section is concerned with a comparison of the data evolved from those studies with that from the present work. In doing so, an attempt is made to define more clearly some alloying and processing principles for carbide strengthened molybdenum alloys.

Figure 29 is a comparison of the ultimate tensile strength of strain hardened molybdenum alloys. The data for Mo-Cb-TZM (ref. 3) and Mo-TZC (ref. 1) represent the strength in the optimum processed condition for each alloy. It can be noted that the strength of MHC-39K-89 is considerably higher than those of the other alloys over the entire temperature range from 1500^o to 3000^o F (1088 to 1922 K). Figure 30 shows the

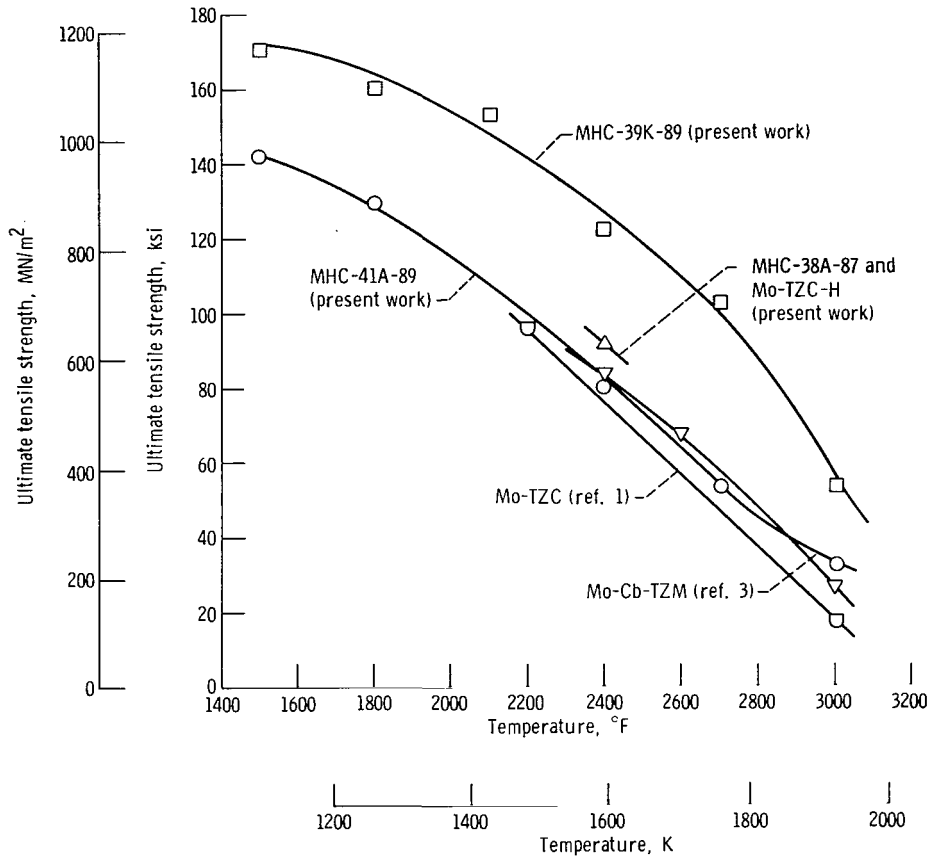


Figure 29. - Ultimate tensile strength as function of temperature for wrought molybdenum alloys.

stress dependency of the rupture life at 2400^o F (1588 K) for a similar series of alloys. For short time tests, of the order of 10 hours, the alloy MHC-39K-89 is the strongest, followed by an alloy developed from the previous study MHC-21A-89 (ref. 6). The situation becomes more complex for rupture times of the order of 100 hours or more. The alloy Mo-Cb-TZM developed by Perkins et al. (ref. 3) begins to lose its strength above 10 hours as a result of recrystallization. The strongest alloy at 100 hours appears to be MHC-21A-89 rather than MHC-39K-89 because of the low stress sensitivity of the rupture life for MHC-39K-89, while the curves for the other alloys are considerably flatter. It can be noted that solution treated and aged Mo-Cb-TZM has a particularly flat stress-rupture - time curve and it may be that for very long times this alloy will show the highest strength.

Figures 29 and 30 show that the alloys developed in this program are among the most attractive molybdenum base alloys both in short time tension tests and in rupture tests (at least under 100-hr duration). It should also be noted that the strongest alloys in the short time tests are not necessarily strongest in long time creep rupture (>100 hr).

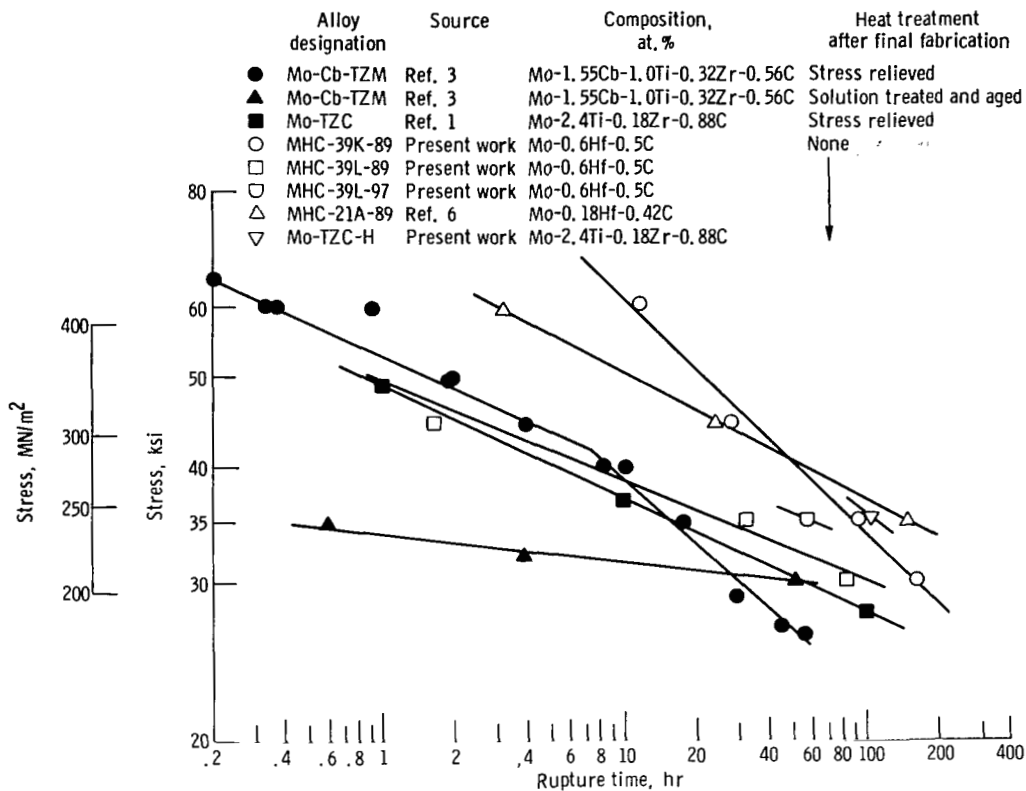


Figure 30. - Stress dependency of rupture time for various molybdenum alloys at 2400° F (1588 K).

It is interesting to compare the various types of processes necessary to produce optimum properties in the various molybdenum alloys. The high strength of the overaged alloys Mo-Cb-TZM and Mo-TZC alloys is derived from a processing schedule similar to the E process utilized in this study. The E process relies on a solution treatment and aging step inserted prior to the final strain hardening process. It was noted previously that such a process did not produce optimum short time properties for the present Mo-Hf-C alloys (see figs. 7(a) and (c)). The reason for this difference may be found in the differences in the precipitation processes for the two types of alloys. Carbide precipitation in molybdenum alloys has been extensively studied by Ryan and co-workers (refs. 21 and 22). They found (in agreement with the earlier work of Chang, ref. 2) that precipitation in Mo-TZC occurs via the conversion of a molybdenum carbide Mo_2C to a mixed titanium-zirconium monocarbide. The Mo_2C is present in the quenched solution treated alloys. A similar reaction occurs in Mo-Cb-TZM where the conversion proceeds from Mo_2C to CbC . The resultant carbide in these alloys is a rather coarse platelet lying on the {001} cube planes of the molybdenum matrix. In contrast, precipitation in the Mo-Hf-C alloys studied in this program occurs directly from solid solution and no Mo_2C is present in the quenched alloys. This condition is met if the Hf/C ratio is between

1 and 1.5 (ref. 21) which was met for MHC-38, 39, and 41, the alloys most extensively studied in this program. The resulting HfC precipitates as smaller platelets, also on the {001} plane.

The different precipitation sequence may also explain the rather pronounced response to dynamic strengthening during swaging exhibited by MHC-39. It was shown earlier (ref. 20) that the flow stress peak in Mo-Zr-C alloys occurs at a higher temperature than it does in Mo-TZC. The precipitation kinetics for ZrC in Mo are similar to those for HfC. It appears then that dynamic strengthening in Mo-Hf-C can occur in the temperature range where swaging of molybdenum alloys is usually performed.

CONCLUDING REMARKS

The present study has identified a series of compositions and thermomechanical processes for producing potentially useful high-temperature materials. Thermomechanical processes for molybdenum base materials have been classified as to whether the carbides are present in the overaged or a metastable condition prior to the final strain hardening step. Apparently the metastable alloys (termed "strain aged") derive their strength from both the precipitation of a carbide during strain hardening and during testing of the strain hardened alloy.

For overaged alloys, the importance of maintaining a small interparticle spacing was emphasized, particularly for good creep resistance. It was pointed out that this small interparticle spacing can arise from a solution anneal and aging treatment prior to the final strain hardening. However, no recrystallization treatments should be given subsequent to this solution and aging reaction because of the possibility of accelerated particle coarsening.

The degree of strain hardening as evidenced by the subgrain size does not appear to be of much importance for long-term creep applications. However, for short-time applications, strain hardening could be the predominant strengthening mechanism.

SUMMARY OF RESULTS

The high-temperature mechanical properties of Mo-Hf-C alloys are extremely sensitive to processing variables. From an electron microscopy study of the microstructure of these alloys, two classes were identified. Overaged alloys are those containing an overaged hafnium carbide precipitate within a strain hardened matrix. The short time tensile strength of these alloys was found to be sensitive to both the hafnium carbide particle size and spacing, and most important, to the average subgrain size produced

during fabrication. The minimum creep rate for the overaged alloys at 2400⁰ F (1588 K) was not a function of the subgrain size. However, a good relation was found between the minimum creep rate and $L^{2.9}$, where L is the interparticle spacing.

Some extremely attractive mechanical properties were obtained in the strain aged alloys. A Mo-0.6 percent Hf-0.5 percent C alloy which was extruded at 4000⁰ F (2477 K) prior to swaging had an ultimate tensile strength greater than 100 ksi (690 MN/m²) over the temperature range 1500⁰ to 2700⁰ F (1088 to 1755 K). These properties resulted from the alloy being in a metastable state prior to swaging. This metastability allowed dynamic strengthening to occur during swaging resulting in the production of an extremely fine particle distribution as well as a unique strain hardened substructure.

Lewis Research Center,
National Aeronautics and Space Administration,
Cleveland, Ohio, October 3, 1969,
129-03.

REFERENCES

1. Semchyshen, M.; Barr, Robert Q.; and Kalns, E.: Arc-Cast Molybdenum-Base Alloys (1962-1964). Climax Molybdenum Co., 1964. (Available from DDC as AD-602432.)
2. Chang, W. H.: Effect of Heat Treatment on Strength Properties of Molybdenum Base Alloys. Trans. ASM, vol. 56, 1963, pp. 107-124.
3. Perkins, R. A.: Effect of Processing Variables on the Structure and Properties of Refractory Metals. Rep. LMSC-2-69-67-1, Lockheed Missiles and Space Co. (AFML-TR-65-234, Pt. 2, DDC No. AD-816137), May 1967.
4. Raffo, Peter L.; and Klopp, William D.: Mechanical Properties of Solid-Solution and Carbide-Strengthened Arc-Melted Tungsten Alloys. NASA TN D-3248, 1966.
5. Rubenstein, L. S.: Effects of Composition and Heat Treatment on High-Temperature Strength of Arc-Melted Tungsten-Hafnium-Carbon Alloys. NASA TN D-4379, 1968.
6. Raffo, Peter L.: Exploratory Study of Mechanical Properties and Heat Treatment of Molybdenum-Hafnium-Carbon Alloys. NASA TN D-5025, 1969.
7. Gyorgak, Charles A.: Extrusion at Temperatures Approaching 5000⁰ F. NASA TN D-3014, 1965.
8. Bobrowsky, A.; and Stack, E. A.: Research on Hydrostatic Extrusion of the TZM Alloy at Ambient Temperature. Pressure Technology Corp. of America (AFML-TDR-64-205, DDC No. AD-607682), June 1964.

9. Ashby, Michael: The Hardening of Metals by Nondeforming Particles. *Z. Metallk.*, vol. 55, 1964, pp. 5-17.
10. Schoone, R. D.; and Fischione, E. A.: Automatic Unit for Thinning Transmission Electron Microscopy Specimens of Metals. *Rev. Sci. Instr.*, vol. 37, no. 10, Oct. 1966, pp. 1351-1353.
11. Gebhardt, Erich; Fromm, Eckehard; and Roy, Upendra: Die Löslichkeit von Kohlenstoff in Molybdän, Wolfram and Rhenium. *Zeit. Metallkde*, vol. 57, no. 10, 1966, pp. 732-736.
12. Rudman, P. S.: The Solubility Limit and Diffusivity of Carbon in Molybdenum. *Trans. AIME*, vol. 239, no. 12, Dec. 1967, pp. 1949-1954.
13. Hirsch, P. B., et al.: *Electron Microscopy of Thin Crystals*. Butterworths Publ., 1965.
14. Ashby, M. F.; and Centamore, R. M. A.: The Dragging of Small Oxide Particles by Migrating Grain Boundaries in Copper. *Acta Met.*, vol. 16, no. 9, Sept. 1968, pp. 1081-1092.
15. Glen, J.: The Effect of Alloying Elements on Creep Behavior. *J. Iron Steel Inst.*, vol. 190, pt. 2, Oct. 1958, pp. 114-135.
16. Raffo, Peter L.: Dynamic Strain Aging During the Creep and Tensile Testing of a Molybdenum-Titanium-Carbon Alloy. NASA TN D-5169, 1969.
17. Embury, J. D.; Keh, A. S.; and Fisher, R. M.: Substructural Strengthening in Materials Subject to Large Plastic Strains. *Trans. AIME*, vol. 236, no. 9, Sept. 1966, pp. 1252-1260.
18. Wilcox, B. A.: Basic Strengthening Mechanisms in Refractory Metals. *Refractory Metal Alloys*. I. Machlin, R. T. Begley, and E. D. Weisert, eds., Plenum Press, 1968, pp. 1-39.
19. Wilcox, B. A.; and Gilbert, A.: Substructural Strengthening of a Precipitation Hardened Molybdenum Alloy. *Acta Met.*, vol. 15, no. 4, Apr. 1967, pp. 601-606.
20. Raffo, Peter L.: Dynamic Strain Aging in Carbide Strengthened Molybdenum Alloys. NASA TN D-5355, 1969.
21. Ryan, N. E.; and Martin, J. W.: The Formation and Stability of Group IV A Carbides and Nitrides in Molybdenum. *J. Less. Common Metals*, vol. 17, no. 4, Apr. 1969, pp. 363-376.
22. Ryan, N. E.; Soffa, W. A.; and Crawford, R. C.: Orientation and Habit Plane Relationships for Carbide and Nitride Precipitates in Molybdenum. *Metallography*, vol. 1, no. 2, Nov. 1968, pp. 195-220.

TABLE I. - COMPOSITIONS OF ALLOYS

Alloy designation	Composition, at. %	Processes studied (see table II)
MHC-38	Mo-0.47 Hf-0.29 C	A, E
MHC-39	Mo-0.60 Hf-0.50 C	K, L
MHC-40	Mo-1.04 Hf-0.30 C	A
MHC-41	Mo-0.99 Hf-0.72 C	A, B, C, D, E, F, G
MHC-42	Mo-1.09 Hf-1.19 C	A
Mo-TZC	Mo-2.4 Ti-0.18 Zr-0.88 C	H

TABLE II. - THERMOMECHANICAL PROCESSES

Process designation	Extrusion temperature		Post-extrusion heat treatment				Swaging temperatures for -			
	°F	K	Solution temperature		Aging temperature		Initial 50 percent reduction		Final reduction	
			°F	K	°F	K	°F	K	°F	K
	A	3500	2200	----	----	----	----	2500	1644	2000
B	↓	↓	----	----	3500 ^a	2200	2500	1644	↓	↓
C	↓	↓	4000	2477 ^b	----	----	2500	1644	↓	↓
D	↓	↓	4000	2477 ^b	----	----	3000	1922	↓	↓
E	↓	↓	4000	2477 ^b	2800	1810 ^c	2500	1644	↓	↓
F	↓	↓	3800	2366 ^a	2800	1810 ^c	2500	1644	↓	↓
G	↓	↓	3800	2366 ^a	2800	1810 ^c	2500	1644	1800	1255
H	(d)	(d)	4000	2477 ^b	----	----	(e)	(e)	(e)	(e)
K	4000	2477	----	----	----	----	2500	1644	2500	1644
L	4000	2477	----	----	2800	1810 ^a	2500	1644	2000	1366

^a60-Min anneal.

^b30-Min anneal.

^c120-Min anneal.

^dMaterial obtained as 0.75-in. (2-cm) swaged rod and further swaged to 0.4 in. (1 cm) at 2500° F (1644 K).

^eHydrostatically extruded 60 percent at room temperature.

TABLE III. - 1-HOUR RECRYSTALLIZATION TEMPERATURES FOR
SELECTED PROCESSING CONDITIONS

Alloy designation	Composition, at. %	Process designa- tion ^a	1-Hr recrystallization temperature, T _r	
			°F	K
MHC-38	Mo-0.47 Hf-0.29 C	A-89	2840	1833
		A-97	2790	1805
		E-89	3230	2050
MHC-39	Mo-0.60 Hf-0.50 C	K-89	2860	1844
		L-89	3210	2040
		L-97	3190	2030
MHC-40	Mo-1.04 Hf-0.30 C	A-89	2640	1722
MHC-41	Mo-0.99 Hf-0.72 C	A-89	3020	1933
		A-97	3000	1922
		B-89	2900	1866
		D-89	3000	1922
		E-89	3240	2055
MHC-42	Mo-1.09 Hf-1.19 C	A-89	3250	2060
Mo-TZC	Mo-2.4 Ti-0.18 Zr-0.88 C	H	2750	1783

^aLetter refers to process designation given in table II; number which follows is percent reduction from extrusion to swaged bar.

TABLE IV. - TENSILE PROPERTIES OF SWAGED ALLOYS

Alloy designation	Composition, at. %	Process designation	Temperature		0.2 Percent offset yield strength		Ultimate tensile strength		Elongation, percent	Reduction in area, percent	
			°F	K	ksi	MN/m ²	ksi	MN/m ²			
MHC-38	Mo-0.47 Hf-0.29 C	A-89	75	300	-----	-----	118.0	816	0	0	
			2400	1588	67.9	469	75.4	520	13	62	
		A-97	2400	1588	75.0	518	91.6	632	7	19	
			E-89	75	300	103.0	709	110.0	761	15	23
		2400		1588	46.7	322	47.5	328	13	60	
		E-97	75	300	135.0	932	146.0	1000	8	40	
			1800	1255	89.4	617	90.7	626	7	91	
			2400	1588	54.7	377	55.7	384	8	69	
3000	1922		28.6	197	29.0	200	16	91			
MHC-39	Mo-0.6 Hf-0.5 C	K-89-1	75	300	176.0	1220	-----	-----	2	2	
			2400	1588	92.2	636	103.0	707	12	63	
		K-89-2	1500	1088	140.0	964	171.0	1180	7	48	
			1800	1255	154.0	1060	161.0	1110	10	66	
			2100	1422	148.0	1020	153.0	1060	10	78	
			2400	1588	116.0	800	122.0	845	14	63	
			2700	1755	99.1	684	102.0	705	14	61	
			3000	1922	49.9	344	52.6	363	17	73	
		L-89	75	300	108.0	747	126.0	869	5	2	
			1800	1255	75.0	518	75.6	522	12	88	
			2400	1588	55.2	381	57.8	399	11	76	
			3000	1922	33.2	229	35.3	244	33	91	
L-97	2400	1588	73.3	506	73.3	506	8	57			
	MHC-40	A-89	75	300	107.0	738	118.0	816	13	12	
1800			1255	92.6	639	94.5	652	11	82		
2400			1588	58.4	403	68.4	472	15	80		
3000			1922	20.2	140	21.0	145	66	>98		
A-97		75	300	167.0	1150	185.0	1280	14	25		
		2400	1588	60.3	416	61.8	426	11	76		
MHC-41		Mo-0.99 Hf-0.72 C	A-89	75	300	164.0	1133	-----	-----	1	1
				1500	1088	114.0	785	142.0	981	10	62
	1800			1255	123.0	847	129.0	889	10	66	
	2400			1588	78.3	540	80.0	552	16	65	
	2700			1755	49.7	343	53.1	366	17	84	
	3000			1922	28.3	195	32.7	226	23	89	
	A-97		75	300	194.0	1340	208.0	1440	10	31	
			2400	1588	78.7	543	81.6	563	8	79	
	B-89		75	300	126.0	866	-----	-----	--	--	
			1800	1255	82.3	568	83.5	576	12	88	
			2400	1588	55.5	383	58.3	402	18	72	
			3000	1922	25.3	175	27.3	188	29	95	
B-97	75	300	153.0	1050	162.0	1120	9	53			
	2400	1588	55.4	382	56.5	390	11	73			

TABLE IV. - Concluded. TENSILE PROPERTIES OF SWAGED ALLOYS

Alloy designation	Composition, at. %	Process designation	Temperature		0.2 Percent offset yield strength		Ultimate tensile strength		Elongation, percent	Reduction in area, percent
			°F	K	ksi	MN/m ²	ksi	MN/m ²		
MHC-41	Mo-0.99 Hf-0.72 C	D-89	75	300	103.0	713	-----	----	5	4
			2400	1588	45.7	315	47.3	326	16	72
		D-97	75	300	134.0	925	148.0	1020	10	31
			2400	1588	53.3	368	53.8	371	7	57
		E-89	75	300	113.0	778	-----	----	10	8
			2400	1588	46.9	324	47.8	330	7	49
			3000	1922	11.6	80	11.6	80	5	1
		E-97	75	300	142.0	981	153.0	1060	10	25
			2400	1588	63.2	436	65.3	451	8	70
		F-89	75	300	111.0	768	122.0	844	11	26
			2400	1588	58.4	403	61.5	424	15	80
		F-97	75	300	164.0	1130	180.0	1240	13	54
2400	1588		64.7	446	67.3	464	11	75		
G-89	75	300	111.0	764	121.0	838	20	39		
	2400	1588	55.3	382	58.0	400	16	80		
G-97	75	300	143.0	984	151.0	1040	7	48		
	2400	1588	65.7	453	66.4	458	12	76		
MHC-42	Mo-1.09 Hf-1.19 C	A-89	75	300	130.0	895	155.0	1070	11	41
			1800	1255	92.9	641	97.3	671	11	83
			2400	1588	58.4	403	62.5	431	16	76
			3000	1922	26.6	184	30.5	210	35	88
		A-97	75	300	191.0	1320	216.0	1490	10	72
			2400	1588	63.3	437	66.2	457	11	83
Mo-TZC	Mo-2.4 Ti-0.18 Zr-0.88 C	H	2400	1588	67.1	463	90.3	623	18	45

TABLE V. - CREEP-RUPTURE PROPERTIES OF SWAGED Mo-Hf-C ALLOYS AT 2400° F (1588 K)

Alloy designation	Composition, at. %	Process designation	Stress, σ		Rupture life, t_r , hr	Minimum creep rate, $\dot{\epsilon}_{m-1}$, sec ⁻¹	Elongation, percent	Reduction in area, percent
			ksi	MN/m ²				
MHC-38	Mo-0.47 Hf-0.29 C	E-89	35	242	13.8	6×10^{-7}	20	>98
		E-97	35	242	10.4	8.8	16	81
MHC-39	Mo-0.6 Hf-0.5 C	K-89-1	30	207	159.0	0.33×10^{-7}	13	79
			35	242	96.1	.8	10	--
			45	311	27.9	3.1	12	78
			60	414	11.7	13	13	69
		L-89	30	207	81	1.4	23	90
			35	242	31.8	4.4	24	85
			45	311	1.6	130	14	91
			35	242	57.8	1.5	12	>98
MHC-40	Mo-1.04 Hf-0.3 C	A-89	35	242	2.2	72×10^{-7}	22	89
MHC-41	Mo-0.99 Hf-0.72 C	A-89	35	242	8.5	11.6×10^{-7}	17	77
		A-97			3.9	28.6	14	76
		B-89			4.8	27.5	24	83
		B-97			21.2	6.4	16	70
		D-89			6.5	22.6	21	62
		D-97			1.6	83.3	15	76
		E-89			12.3	10.7	27	78
		E-97			29.5	3.5	20	28
MHC-42	Mo-1.09 Hf-1.19 C	A-89	35	242	2.5	61×10^{-7}	24	82
		A-97	35	242	8.5	9.9	13	73
Mo-TZC	Mo-2.4 Ti-0.18 Zr-0.88 C	H	35	242	106	1.0×10^{-7}	14	54

TABLE VI. - INFLUENCE OF ANNEALING ON CREEP RUPTURE

PROPERTIES OF MHC-38E-89, Mo-0.47 PERCENT

Hf-0.29 PERCENT C, AT 2400° F (1588 K) AND 35 ksi (242 MN/m²)

1-Hr annealing temperature		Rupture life, t_r , hr	Minimum creep rate, $\dot{\epsilon}_{m-1}$, sec ⁻¹	Rupture ductility	
°F	K			Elongation, percent	Reduction in area, percent
As swaged	As swaged	13.8	6.0×10^{-7}	20	>98
2250	1505	6.8	14.0	11	65
2500	1644	8.7	13.0	24	89
2750	1783	15.1	4.7	17	91
3000	1922	3.0	18.0	16	94
3250	2060	0.01	-----	17	>98
3500	2200	50.	0.42×10^{-7}	16	82
4000	2477	39.1	.33	7	11

TABLE VII. - YIELD STRESSES AND SUBGRAIN SIZES OF Mo-Hf-C ALLOYS

Alloy designation	Composition, at. %		Average subgrain diameter, d , μm	$d^{-1/2}$, $(\mu\text{m})^{-1/2}$	0.2 Percent offset yield stress			
	Hf	C			Room temperature		2400 ^o F	1588 K
					ksi	MN/m ²	ksi	MN/m ²
^a MHC-20 A-89	0.09	0.24	1.20	0.91	115	791	57.3	395
^a MHC-21 A-89	.18	.42	.63	1.26	121	834	68.9	475
^a MHC-22 A-89	.37	.29	.47	1.46	134	925	65.2	450
^a MHC-23 A-89	.39	.65	.49	1.43	139	960	67.7	467
^a MHC-26 A-89	.37	.89	.71	1.19	130	898	61.5	424
MHC-38 A-97	.47	.29	.44	1.51	---	----	75.0	518
^a MHC-24 A-89	.58	.77	.65	1.24	130	899	61.7	425
MHC-39 K-89	.60	.50	1.20	.91	176	1210	92.2	636
MHC-39 L-89	.60	.50	.59	1.30	108	745	55.2	381
MHC-39 L-97	.60	.50	.49	1.43	---	----	73.3	506
MHC-40 A-97	1.04	.30	.53	1.37	166	1150	60.3	416
MHC-41 A-89	.99	.72	.58	1.31	164	1130	78.3	540
MHC-41 A-97	↓	↓	.40	1.58	194	1340	78.7	543
MHC-41 E-89	↓	↓	.93	1.04	113	780	46.9	324
MHC-41 E-97	↓	↓	.55	1.35	142	980	63.2	436
MHC-41 F-89	↓	↓	.54	1.36	111	766	58.4	403
MHC-41 F-97	↓	↓	.44	1.51	164	1130	64.7	446
MHC-41 G-89	↓	↓	.59	1.30	111	766	55.3	382
MHC-41 G-97	↓	↓	.34	1.71	143	987	65.7	453
MHC-41 D-89	↓	↓	.79	1.13	103	711	45.7	315
MHC-41 D-97	↓	↓	.56	1.34	134	925	53.3	368
MHC-41 B-89	↓	↓	.61	1.28	126	869	55.5	383
MHC-41 B-97	↓	↓	.52	1.39	153	1056	55.4	382
^a MHC-25 A-89	.96	.82	.62	1.27	145	997	64.2	443
^a MHC-27 A-89	.98	1.11	.45	1.49	155	1070	73.6	507
MHC-42 A-89	1.09	1.19	.44	1.51	130	897	58.4	403
MHC-42 A-97	1.09	1.19	.44	1.51	191	1318	63.3	437
^a MHC-28 A-89	1.83	1.07	.54	1.36	132	910	56.1	387

^aYield strengths of these alloys were originally reported in ref. 6.

FIRST CLASS MAIL



POSTAGE AND FEES PAID
NATIONAL AERONAUTICS A
SPACE ADMINISTRATION

000 001 42 01 305 70033 00104
AIR FORCE AIRCRAFT LABORATORY WADWELL
WRIGHT-PATTERSON AFB OHIO 45433

OFFICIAL BUSINESS PENALTY FOR PRIVATE USE \$300

POSTMASTER: If Undeliverable (Section 15
Postal Manual) Do Not Return

"The aeronautical and space activities of the United States shall be conducted so as to contribute . . . to the expansion of human knowledge of phenomena in the atmosphere and space. The Administration shall provide for the widest practicable and appropriate dissemination of information concerning its activities and the results thereof."

— NATIONAL AERONAUTICS AND SPACE ACT OF 1958

NASA SCIENTIFIC AND TECHNICAL PUBLICATIONS

TECHNICAL REPORTS: Scientific and technical information considered important, complete, and a lasting contribution to existing knowledge.

TECHNICAL NOTES: Information less broad in scope but nevertheless of importance as a contribution to existing knowledge.

TECHNICAL MEMORANDUMS: Information receiving limited distribution because of preliminary data, security classification, or other reasons.

CONTRACTOR REPORTS: Scientific and technical information generated under a NASA contract or grant and considered an important contribution to existing knowledge.

TECHNICAL TRANSLATIONS: Information published in a foreign language considered to merit NASA distribution in English.

SPECIAL PUBLICATIONS: Information derived from or of value to NASA activities. Publications include conference proceedings, monographs, data compilations, handbooks, sourcebooks, and special bibliographies.

TECHNOLOGY UTILIZATION PUBLICATIONS: Information on technology used by NASA that may be of particular interest in commercial and other non-aerospace applications. Publications include Tech Briefs, Technology Utilization Reports and Notes, and Technology Surveys.

Details on the availability of these publications may be obtained from:

**SCIENTIFIC AND TECHNICAL INFORMATION DIVISION
NATIONAL AERONAUTICS AND SPACE ADMINISTRATION
Washington, D.C. 20546**